

The Challenges and Possibilities of a Truly Quiet Helicopter

29th Alexander A. Nikolsky Honorary Lecture



Fredric H. Schmitz*

*Senior Research Professor**Department of Aerospace Engineering
University of Maryland, College Park, MD*

The important noise sources for rotary winged aircraft are reviewed and ranked, with an emphasis on the single-rotor helicopter. Harmonic noise from both the main rotor and tail rotor are the dominant noise sources for both military and civilian applications. Noise radiation patterns for hover and forward flight are illustrated and compared with simple noise radiation modeling to provide insight as to the origins of harmonic noise radiation. Harmonic rotor noise due to the thickness of the rotor blade near the blade tip has been shown to have a strong dependence on rotor tip Mach number. An extreme form of harmonic noise, high-speed impulsive noise, can occur when the advancing tip Mach number of the advancing rotor approaches 1.0—causing the local flow near the tip of the rotor to delocalize. Harmonic noise radiation has also been shown to be dependent on steady and unsteady rotor blade loading. Strong unsteady blade loadings occur when the rotor blades pass in close proximity to the blade wake, causing blade–vortex interaction (BVI) noise. Simple radiation patterns for BVI have confirmed the importance of the trace Mach number in setting the directivity and level of BVI noise radiation. Several ways of reducing and canceling radiated noise are reviewed and compared with experiment and current practice, including acoustic design, flight path management, and active acoustic cancellation. Promising research and development directions are suggested that offer additional noise reduction gains.

Introduction

Helicopter noise is an inevitable by-product of creating the lift necessary to make the helicopter and other rotor/propeller vertical lift machines work. Rotor blades in effect accelerate the air as they pass over fixed positions in space in close proximity to the blade. This acceleration also causes equal and opposite forces (lift and drag) on the blade that determine rotor performance. The finite thickness of each blade also causes a local acceleration and net displacement of the air surrounding each blade. Both of these effects cause compressible waves, originating at the rotor blades, to radiate noise to an observer far from the noise source. The basic physics of these phenomena has been known for more than six decades (for more than a century, for propellers).

It is intuitive that heavier vertical takeoff and landing (VTOL) aircraft are generally noisier than small ones because generating more lift in hover requires more air to be accelerated. Momentum theory also tells us that the most efficient way of generating that lift in hover is to accelerate a large amount of air as slowly as possible—or keep the ratio of thrust per unit area (disk loading) and hence the induced velocity of the rotor systems as small as possible (Ref. 1). This fact is shown qualitatively in Fig. 1 for all types of VTOL vehicles. In general, pure jet VTOLs are noisier than helicopters. Figure 2 shows a similar trend for some older

Army helicopters. Note that the noise is measured in perceived noise using a decibel (dB) scale (PNdB). This metric attempts to represent human annoyance of the noise and was developed primarily for jet noise—but it has been used to measure the annoyance of rotorcraft noise as well.

It is also known that a rotor's tip Mach number (tip speed of the rotor divided by the local speed of sound) is a powerful parameter when it comes to noise radiation. Sound, which is a radiating pressure fluctuation, travels at the local speed of sound with respect to the medium it is traveling through. When sources of sound are moving close to the sound speed, the perturbation pressures surrounding the moving source effectively become larger ahead of the moving source and can increase the intensity of the radiating noise quite dramatically for positions ahead of the rotating blades. So for a fixed disk loading and size, rotors that have low tip Mach numbers are generally quieter than rotors with high tip Mach numbers (Refs. 1–3).

It is also intuitive that operating a rotor in undisturbed air will create less noise than one operating in turbulent air. The turbulent air causes local changes in blade loading that cause local unsteady disturbances to radiate as additional noise. So it is important to have rotors operate in as clean an inflow as possible. This usually implies that each rotor be designed and operated to avoid disturbance fields from other components on the rotorcraft and from the disturbance field generated by its own wake (Refs. 4–6).

However, having qualitative knowledge about the general phenomena is not sufficient to design a quiet helicopter. Such was the fate of the U.S. Army's 1960s era "Quiet Helicopter Program." During the Vietnam War,

*Corresponding author; email: fschmitz@umd.edu.
Manuscript received July 2016; accepted July 16.

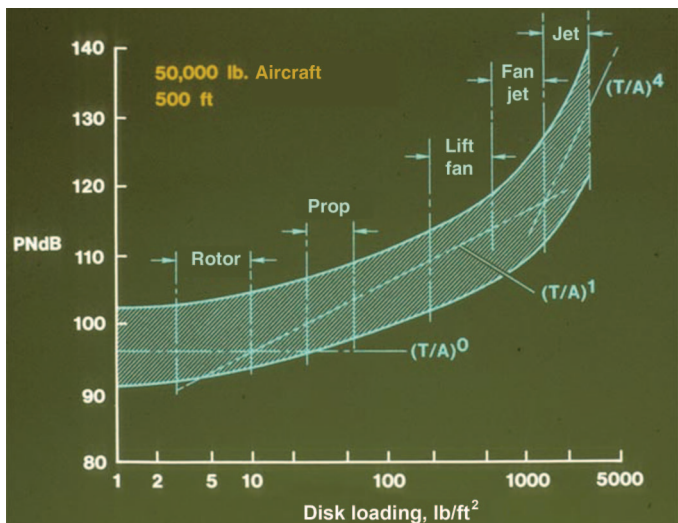


Fig. 1. Vertical lift noise level trends.

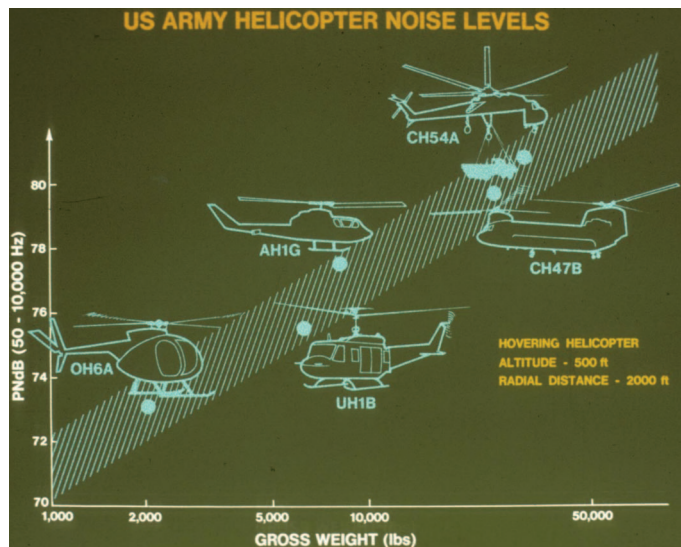


Fig. 2. U.S. Army helicopter noise level trends.

it was noticed that the Army was losing too many helicopters to ground fire and that part of the reason for these losses was that the enemy could hear the approaching helicopters long before they became visible. The Defense Research Project Agency (DARPA) decided to initiate an experimental research program to address the noise problem, and several of the major manufacturers of helicopters were given contracts to substantially reduce helicopter noise.

Hughes Helicopters performed one of the more successful programs for the OH-6A turbine powered helicopter (Ref. 7). In hover, it was discovered that tail rotor noise was the dominant noise source for the OH-6A, followed by engine noise, and then, main rotor noise. In forward flight, the harmonic noise from the main rotor became more important than engine noise. It was demonstrated that engine noise could be reduced with a good muffler, at the expense of additional weight and with some loss of engine performance. Lowering helicopter tip speeds (effectively lowering the tip Mach numbers) of both the main rotor and tail rotor, thus reducing tail rotor noise and main rotor noise. (The main rotor transmission in this helicopter had enough design margin to tolerate the increase in torque due to the reduced tip speed.) To maintain lifting

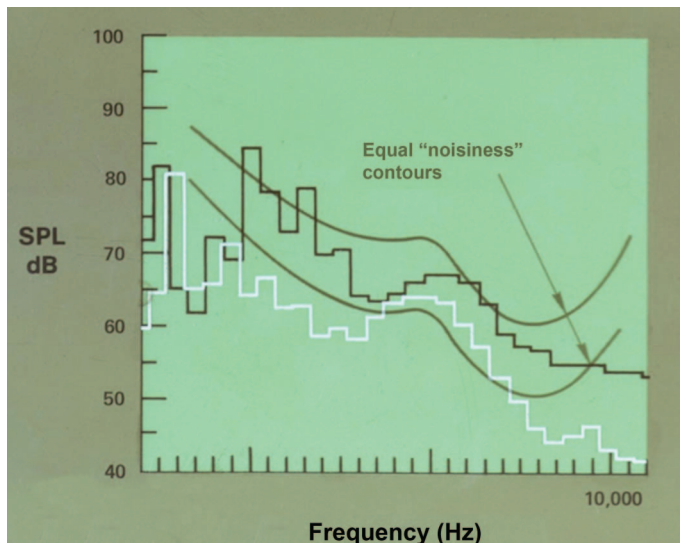


Fig. 3. Measured noise levels in hover of the Standard & Quiet OH-6A Helicopter.

performance of the OH-6A at these lower tip speeds, a fifth blade was added to the normally four-bladed configuration. A higher solidity four-bladed tail rotor was also added, replacing the two-bladed design, to produce the required torque at these operational speeds. These sources of noise and the noise reductions for each source are plotted in Fig. 3 as a function of frequency.

Superimposed on Fig. 3 are the equal noisiness contours at low-to-moderate frequency, as perceived by the human observer. In general, a high level of low-frequency noise is seen to yield the same annoyance as a lower level of medium frequency sound. This human observer characteristic is why the higher frequency tail rotor noise can often be much more annoying than low-frequency main rotor noise sources. However, detection by a far-field observer depends more on the low-frequency nature of rotorcraft noise because low-frequency sound can propagate long distances with minimum atmospheric attenuation. Main rotor low-frequency noise determines the audible detection distance of many helicopters.

In a follow-on program supported by the U.S. Army, these noise reductions were confirmed by measuring each noise source independently (Ref. 8). It was also discovered that while this general knowledge was helpful, it could not be universally applied to reduce the noise of the other operational helicopters of that era. Sacrificing lift by reducing tip speed was not a viable option because the helicopters were already marginal performers in the high-temperature environment of Vietnam. Adding the extra weight necessary for extra blades, increasing torques, and engine mufflers were not acceptable solutions. It was realized that reducing noise would probably have to come at some performance sacrifice and that a detailed knowledge of how noise was generated would be required to make the necessary engineering trade-offs.

Helicopters that had rotors turning at high tip speeds were extremely noticeable or detectable—especially on cold days—thus confirming the strong dependence of noise on tip speed (tip Mach number). The UH-1H helicopter produced a very noticeable and detectable impulsive sound signature that occurred during descent and during high-speed forward flight. Wind tunnel and flight tests confirmed these findings, but the detailed understanding and modeling of these events were not available. Part of the problem was the data analysis technology of that time. Data were recorded on high-speed tape machines and analyzed using analog frequency domain instrumentation. In most instances, an analysis was made of the sound power of the noise versus frequency—where the phase

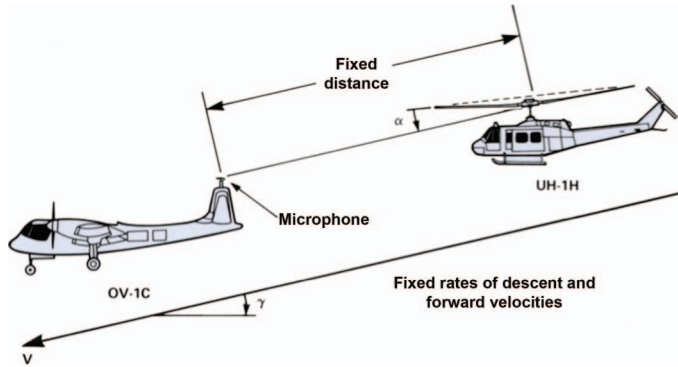


Fig. 4. In-flight Station-Keeping Noise Measurement Program.

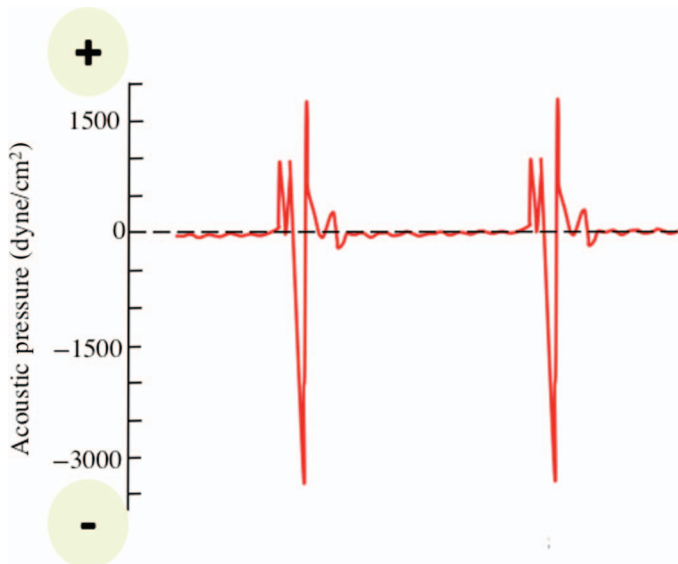


Fig. 5. Pulse shape for UH-1H helicopter for an in-plane microphone.

of these impulsive events was ignored. Simply noting that impulsive noise contained high harmonics of the measured noise in the frequency domain helped identify impulsive noise—but this information alone was not sufficient to quantitatively determine its origins.

The author introduced a novel method of measuring noise on helicopters and employed time domain analysis techniques in the late 1970s that led to a more quantitative understanding of the sources of helicopter impulsive noise (Ref. 9). The essence of this idea is shown in Fig. 4. A quiet fixed wing aircraft was flown in formation with the subject helicopter at a chosen steady-state flight condition. The fixed wing aircraft was outfitted with one or more microphones (one in this case, on the tail of the OV-1C aircraft) to measure the noise radiated by the helicopter. The helicopter was flown, in formation with the fixed wing aircraft, to specified positions with respect to the microphones. When the chosen flight condition was stabilized, data were recorded. By repeating these measurements at many measurement positions, the directivity of the radiated noise was quantitatively determined. The data were gathered and stored in the time domain so that important phase information was not lost in the analysis. Aerodynamic events that occurred on the rotor blades were correlated with the measured acoustic time histories to help explain different sources of impulsive noise. The measured acoustic data proved invaluable for validating first principle acoustic predictions.

Conditions were chosen to explore the governing physics of the impulsive noise phenomena: For the UH-1H, a steady-state descent at 80 kt indicated airspeed (KIAS) and 400 ft/min rate of sink, and high-speed level flight at 115 KIAS. Figure 5 shows a composite sketch of a typical time history containing the major features of the measured data. One complete revolution of rotor time is shown corresponding to about 0.2 s of data. It is apparent that the signal repeats twice per revolution with each distinct pulse corresponding to the signal radiated by each rotor blade. The character of the pulse is seen to consist of some narrow positive pressure spikes followed closely by a relatively large negative pressure pulse. The narrow positive pressure spikes are known to be due to blade–vortex interaction (BVI), whereas the large negative pressure pulse is due to rotor blade thickness. At very high advancing tip Mach numbers, an extreme case of thickness noise, called high-speed impulsive (HSI) noise, occurs when the local transonic aerodynamic flow field extends off the tip of the blade and connects to the acoustic far field. This phenomenon is called “delocalization” and, when it occurs, can be observed in the acoustic measurements as a steep rise in the negative noise pressure peak immediately followed by a discontinuous rise in acoustic pressure on the pressure recovery side of the thickness noise pulse.

Figures 6 and 7 show the advancing side longitudinal and lateral radiation patterns of the UH-1H for the 80 KIAS in descent at 400 ft/min. It is apparent that helicopter impulsive noise is very directional in character. The negative pulse associated with thickness noise is a maximum near the plane of the rotor in the direction of forward flight. It is reduced markedly as an observer moves out of the rotor’s tip-path-plane, reducing to $\frac{1}{2}$ its peak value at 45° under the rotor and becoming almost too small to measure directly under the rotor disk as shown in Fig. 6. Thickness noise is also reduced from its peak value as the observer moves laterally in the plane to the rotor’s 90° azimuth position. BVI pressure spikes are also seen on these figures becoming a maximum near the 30° – 45° longitudinal position.

Figures 8 and 9 show the directivity of helicopter impulsive noise in high-speed forward flight at 115 KIAS. No BVI pulses are observed indicating that BVI at this flight condition is much smaller than the large negative peak due to thickness noise. While the directivity of thickness noise remains similar to the low-speed descent case, its character changes markedly. Near the plane of the rotor in the direction of forward flight, the thickness noise pulse becomes more saw-toothed. The negative thickness noise pulse amplitude grows, and the peak low pressure is followed by a shock wave—radiating large amounts of acoustic energy. In essence, the transonic aerodynamic effects on the rotor have “delocalized” and have caused the local rotor transonic flow field to radiate shocks that originate near the blade tip to the far field observer. When HSI noise is present, it dominates the measured acoustic signatures.

These early measurements, first gathered by the Army using an OV-1C Mohawk fixed wing aircraft as the acoustic measurement platform, redirected many of the research efforts of that period. Previously, it was thought that linear acoustic theory could adequately model the noise of helicopters in high-speed forward flight. The changing pulse shape of HSI noise that was measured in these in-flight test programs was a first indication that something more was happening that was not being captured by then current theories of rotors operating at high tip Mach numbers. In addition, these measurements clearly separated impulsive noise into distinct pulse shapes and tied them to separate aerodynamic events on the rotor.

Many more helicopters were measured with this novel measurement technique and used together with extensive wind tunnel measurements to help verify scaling of rotor noise and to help refine theoretical modeling approaches to both BVI, thickness, and HSI noise radiation (Refs. 10–15). The OV-1C was replaced with a quieter fixed-wing aircraft, the YO-3A, a specially designed quiet aircraft that was developed

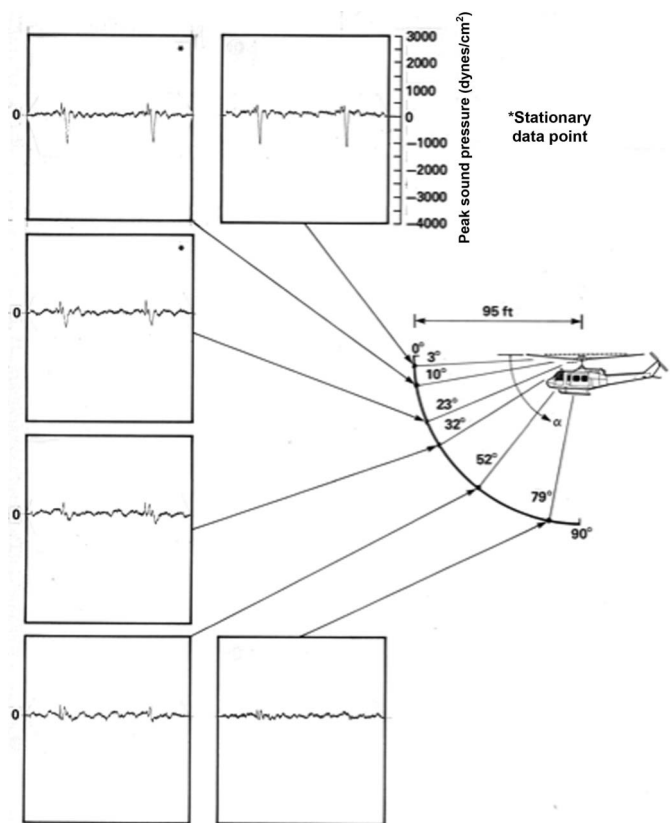


Fig. 6. Longitudinal directivity of UH-1H helicopter, 400 fpm, 80 kt.

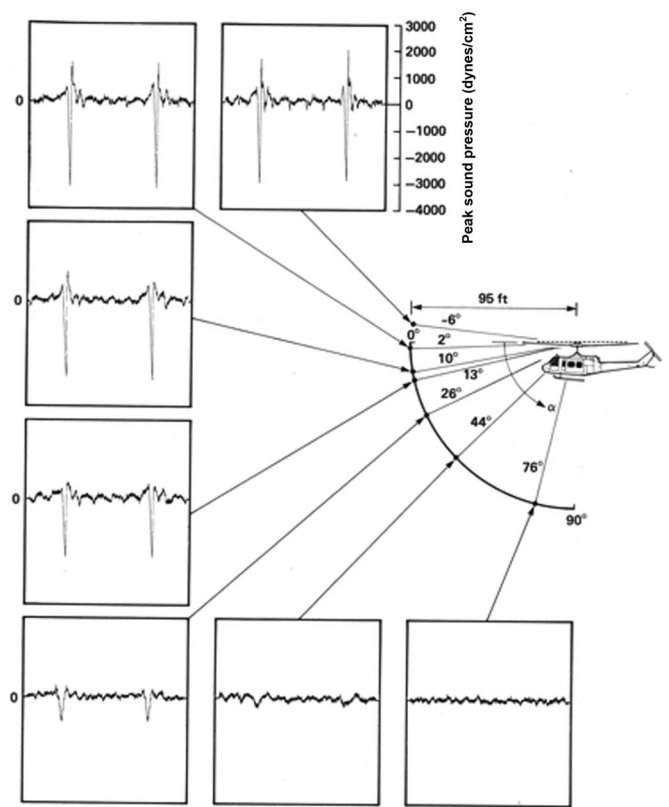


Fig. 8. Longitudinal directivity of UH-1H helicopter flying in high-speed level flight, 115 kt, side view.

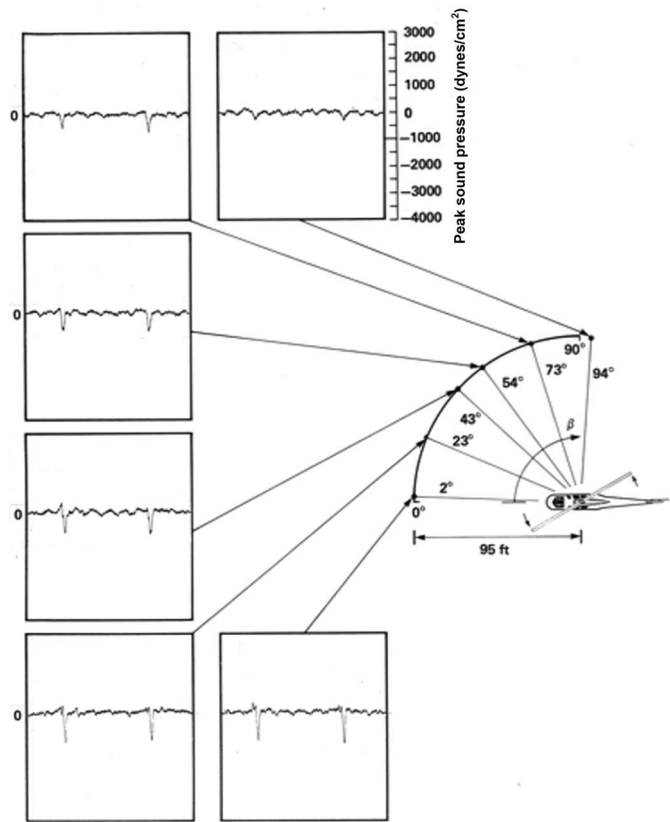


Fig. 7. Lateral directivity of UH-1H helicopter, 400 fpm, 80 kt.

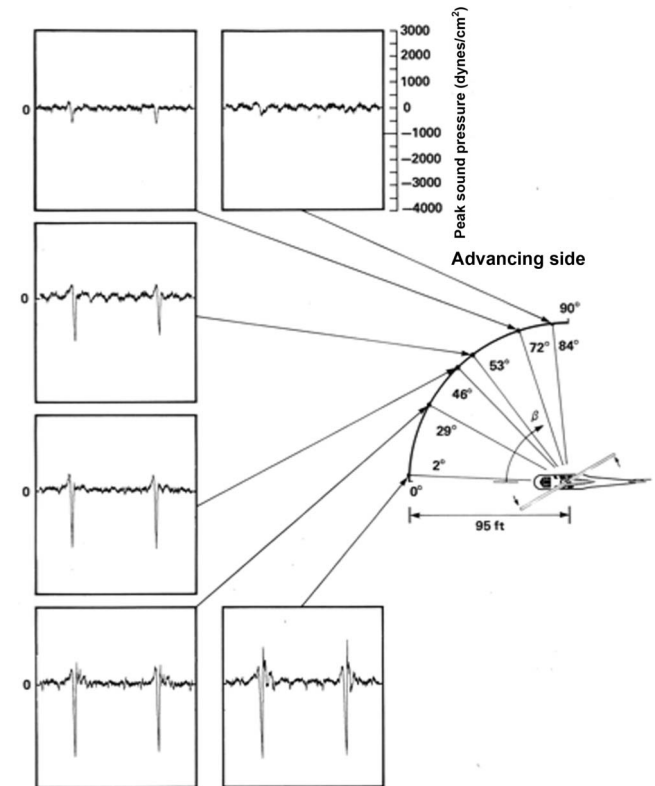


Fig. 9. Lateral directivity of UH-1H helicopter flying in high-speed level flight, 115 kt, top view.



Fig. 10. FBI YO-3A quiet noise measurement platform.



Fig. 11. In-flight YO-3A noise measurement of SSEB prototypes.



Fig. 12. AH-1G in-flight tip shape acoustic measurements.

by Lockheed and used in Vietnam for surveillance. The YO-3A, (Fig. 10), had lower background noise levels than the OV-1C and enabled the collection of better quality acoustic data (Ref. 16).

Obtaining the use of and transforming the YO-3A into an acoustic measurement platform is an interesting story by itself. Although produced in only limited numbers toward the end of the Vietnam War, the FBI had acquired one and was using it for surveillance in the Los Angeles area. My wife, knowing that I was involved in developing this new measurement technique, discovered an article on the YO-3A in a national newspaper and suggested that it might be useful in my research at the Army. After two phone calls, I arranged to meet Mr. Vance Duffy, the director, operations manager, and chief pilot of the FBI's Los Angeles aerial surveillance unit. Together, we initiated a new testing program that utilized the FBI's YO-3A as the acoustic measurement platform that provided unique in-flight acoustic data on a whole series of helicopters.

Acoustic data from the new method were used during two Army Source Selection and Evaluation Boards (SSEBs) to determine the acoustic signature for the Utility Tactical Transport Airborne System (UTTAS) and the Advanced Attack Helicopter (AAH). A view from the cockpit of the helicopter being tested is shown in the upper portion of Fig. 11. The winner of the UTTAS competition is shown flying in formation with the FBI's quiet YO-3A aircraft on the right side of Fig. 11, whereas the losing entry of the AAH competition, the AH-63 helicopter, is shown on the left side of the same figure. In a later testing program with a NASA-owned YO-3A, the same method was also used to determine the acoustic effectiveness of some novel blade shapes as shown in Fig. 12. Both the trapezoidal tip Improved Main Rotor Blades (IMRB) shown on the left and the Ogive shaped tip (OGEE) shown on the right reduced BVI noise substantially (3–5 PNdb) over the square tipped AH-1 rotor blades and reduced the in-plane thickness noise peak levels by up to 6 dB at the same forward airspeeds (Ref. 17). In addition, the IMRB blades attained 10 more knots of forward flight speed at the same power. Unfortunately, hover performance was degraded at high lift for both of the OGEE and IMRB blade designs.

Helicopter Noise

Before we try to understand the origins and mechanisms of helicopter external noise, it is instructive to try to classify and note the most objectionable or noticeable sources. In general, each rotorcraft configuration will have different types of noises associated with their particular design: i.e., single-rotor helicopters with tail rotors, tandem rotor helicopters with overlapping lifting rotors, tiltrotor aircraft with side-by-side lifting rotors that provide lift in hover and propel the aircraft in forward flight. For this paper, the noise sources associated with a single-rotor helicopter that uses a tail rotor for directional control is considered to be most representative. This configuration is ubiquitous throughout the industry and has many of the noise sources that are present in the other configurations. The relative order of importance in terms of producing an acceptably quiet helicopter is shown in Fig. 13 for a generic single-rotor helicopter (Refs. 2–6). In the following sections, the physics that cause each source of noise will be discussed. A book chapter by the author was published in 1996 covers similar material from a slightly different point of view (Ref. 18). (It should be noted that new technology is being used to attack many of these sources resulting in much quieter helicopters today and holds the potential for even further quieting.)

Impulsive harmonic noise usually dominates helicopter detectability and annoyance for both the main rotor and tail rotor. The tip region on the advancing side of the rotor near the 90° azimuth angle of the rotor disk, often produces most of the radiated harmonic noise. As discussed previously, the high advancing Mach numbers in this region amplify the thickness and loading noise sources on each blade element. At very

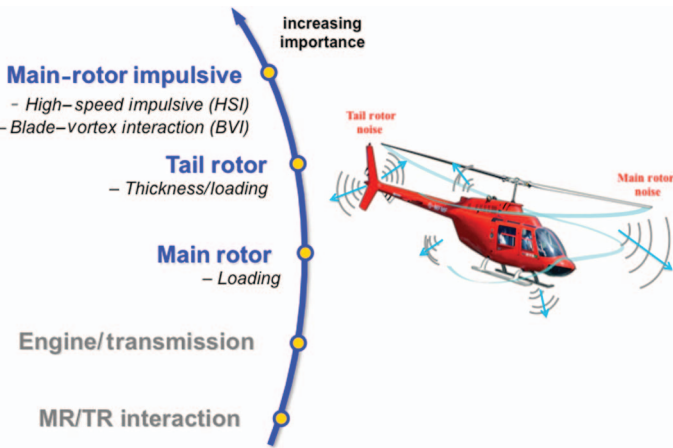


Fig. 13. Relative importance of helicopter acoustic noise sources.

high advancing tip Mach numbers, a change in the acoustic waveform occurs—becoming more saw-toothed in character and the radiated noise is called HSI noise. HSI noise is almost always intolerable and detectable and dominates the acoustic signature of the helicopter. This type of noise tended to dominate the main rotor noise of the “Huey” helicopter of the Vietnam War era. Today, most modern helicopters are designed so that “delocalization” does not occur for normal operations.

A second impulsive noise is present on most helicopters is caused by sudden, rapid pressure changes occurring on the lifting rotor blades. These pressure fluctuations (occurring when the rotors pass in close proximity to their previously shed or trailed tip vortices) normally happen when the helicopter is operating in descending or decelerating flight, when the rotor blades are passing through or near their own wake system. This “wop-wop” sounding impulse stream, called BVI, is often the characteristic sound that distinguishes helicopter operational noise from other transportation noise sources in the terminal operations area.

The noise produced by the antitorque device of a single-rotor helicopter can also be an important noise source. When tail rotors are the antitorque device (as depicted in Fig. 13), the dominant sources are fundamentally the same as the main rotor. However, the higher operating RPM of the tail rotor increases the lower and midfrequencies and make harmonic noise more noticeable and objectionable to a far-field observer. Because the tail rotor is often unloaded in forward flight, tail rotor thickness noise can often be the first sound heard by a far-field observer located along the helicopter’s flight path.

The lower frequency harmonic loading of the helicopter is next in order of acoustic importance. This sound is a direct result of the lift and drag (torque) produced by the helicopter and tends to be most important, for civilian helicopter operations, directly underneath the helicopter. However, for the military, the low- to midfrequency radiated noise near the plane of the rotor is of prime concern—because it is not attenuated by the atmosphere and often sets the aural and electronically aided detection distance of the helicopter.

Engine noise can also be important and is a function of engine choice and installed acoustic treatment. Modern turbine engine technology has gotten significantly quieter and is often used in medium-to-large helicopters. Piston-driven helicopter noise can be a problem for small helicopters that are often used for training and personal use. Mufflers and other acoustic treatments can reduce external noise radiation, but at the price of performance and cost.

Transmission noise is important in close proximity to the helicopter or internally, but unless excessive is not usually an external noise problem. On some helicopters in some operating conditions, the main rotor wake

can pass in close proximity to the tail–rotor disk and cause unacceptable increases in noise level. The problem has been minimized by more careful design and operation.

Last on the list of noise sources (although not shown in Fig. 13) is “broadband” noise (Refs. 19–21). Although there have been many definitions of just what this source of noise is and its origins, it does exist. It is caused by changes in localized pressures on the blade caused by aperiodic and/or random unsteady disturbances. It is normally of lower level on light-to-medium weight helicopters with normal operational tip Mach numbers. Broadband noise becomes more important on heavy helicopters as the design tip Mach numbers are lowered, and the number of rotor blades is increased and when the helicopter is overhead or flies away from the observer.

Rotor Harmonic Noise Radiation

Wave radiation patterns of rotors in nonaxial flight

One of the more interesting aspects of helicopter impulsive noise is tying existing theory to the inherent character of the radiating noise. Early measurements were often viewed in the frequency domain where the phase of the pulse shapes was not retained. It is well known that deterministic harmonic noise can be equally well described in the frequency or time domains if the phase of each harmonic is retained (Fig. 14). However, just looking at the frequency distribution of the noise (not considering the phase) tends to limit our understanding of the governing physics. As we have seen, thickness noise has a dominant negative pulse shape, whereas BVI impulsive noise consists of a series of more narrow positive and negative pressure pulses. Using this information, the nature of these pulses can be traced using acoustic theory and leads to a better understanding of the noise generated by open rotors.

The fundamental conservation laws of mass and momentum govern how small waves are radiated in three-dimensional space. Using classical theory in a fixed space coordinate system, the equation of mass and momentum in elemental form are as follows:

$$\begin{aligned} \text{Mass} \quad & \frac{\partial \rho}{\partial t} + \nabla \cdot (\rho \vec{V}) = 0 \\ \text{Momentum} \quad & \frac{\partial(\rho \vec{V})}{\partial t} + \nabla \cdot (\rho \vec{V} \otimes \vec{V}) = -\nabla p \end{aligned}$$

Considering only small perturbations, these equations become

$$\begin{aligned} \Delta \text{Perturbation Mass} \quad & \frac{\partial \rho'}{\partial t} + \rho_0 \nabla \cdot \vec{V}' = 0. \\ \Delta \text{Perturbation momentum} \quad & \rho_0 \frac{\partial \vec{V}'}{\partial t} = -\nabla p'. \end{aligned}$$

Introducing the speed of sound for small disturbances, $a_0^2 = p'/\rho'$.

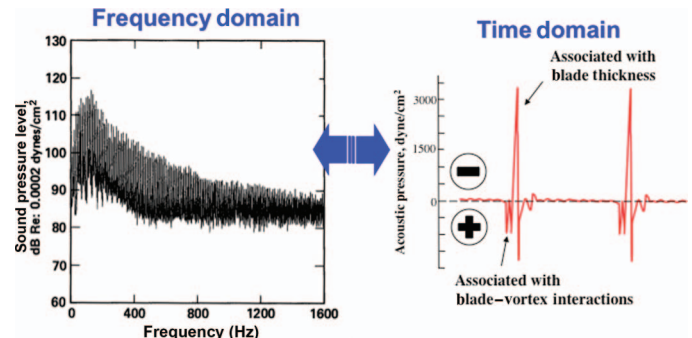


Fig. 14. Equivalence between frequency and time domain analyses.

Taking the time derivative of the perturbation continuity equation and the spatial derivative of the perturbation momentum equation and then subtracting, we obtain the classical small perturbation wave equation:

$$\nabla^2 p' \frac{1}{a_0^2} \frac{\partial^2 p'}{\partial t^2} = 0 \quad (1)$$

Following classical solution techniques, only outgoing waves (waves moving away from the source) are considered. The general fixed space far-field solution for a stationary source in three-dimensional space becomes

$$p' = f \left(t - \frac{r}{a_0} \right) / r \quad (2)$$

where (\cdot) indicates the acoustic pressure at a retarded time, $(\tau = t - \frac{r}{a_0})$.

Notice that the outgoing waves decay inversely proportional to the distance from the source to the observer and that the function, f , needs to be defined by choosing appropriate boundary conditions.

To explain the wave propagation physics of a single-rotor blade in a simple manner, consider the radiation physics of a simple point source—whose boundary conditions could be specified by the finite thickness of a blade panel or by a point force acting on the fluid.

For a stationary source, a small amplitude three-dimensional wave (wavelet) is emitted at an emission time, τ , and travels uniformly at the speed of sound, a_0 , in all directions from this point source. For this example, the form of the equation is

$$p' = \text{Source strength} \left(t - \frac{r}{a_0} \right) / r$$

Now consider a sequence of sound sources that emit wavelets at discrete intervals of time at the same stationary position in space. The sequence of wavelets travels outward from the source in ever expanding circles. The radius of each circle is the speed of sound times the observer time minus the time the wavelet began. The radiating part of these three-dimensional wavelets decays inversely to their distance from their origin as sketched in two-dimensions in Fig. 15. To a fixed observer at a point far from the source, the pressure disturbances arrive at the same equal time intervals. The amplitude of the pulse is the same in all directions when the observer is at a constant distance from the noise source. An example of what this wave pattern might look like can be depicted by imagining small pebbles being dropped into a lake at one location at specific intervals of time and watching circular wavelets propagate away from the point of origin of the wave. Wavelets are seen to propagate out from the source uniformly in all directions. (Note that this water wave analogy, while useful, is not rigorous because surface water waves are transverse waves, whereas acoustic waves are longitudinal waves.)

A noise source moving in a straight line at a constant subsonic velocity, V , is sketched in Fig. 16. In the reference frame attached to the moving source, the flow near the source is steady and obeys the steady-state fluid mechanics equations. However, at fixed spatial positions in close proximity to the moving source, an unsteady disturbance field is created in the stationary medium. At equal time intervals, the moving noise source initiates a sequence of disturbances that act along a line in the direction of the moving source. As in the case of the stationary source, each wavelet obeys the fixed space wave equation but radiates from different positions along the source trajectory. The resulting wave pattern changes dramatically (Fig. 16). The waves ahead of the point source are grouped more closely together (effectively increasing their frequency and amplitude), whereas those in the opposite direction are wider apart (effectively decreasing their frequency and amplitude). This

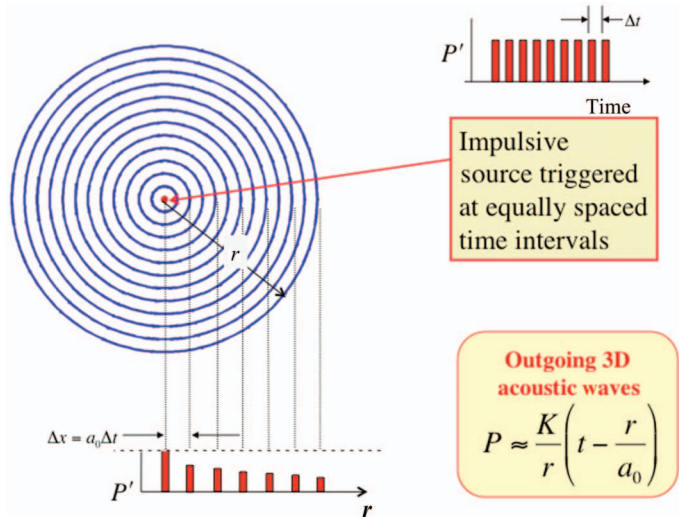


Fig. 15. Two-dimensional cross section of a wavelet pattern from a stationary point source pulse train.

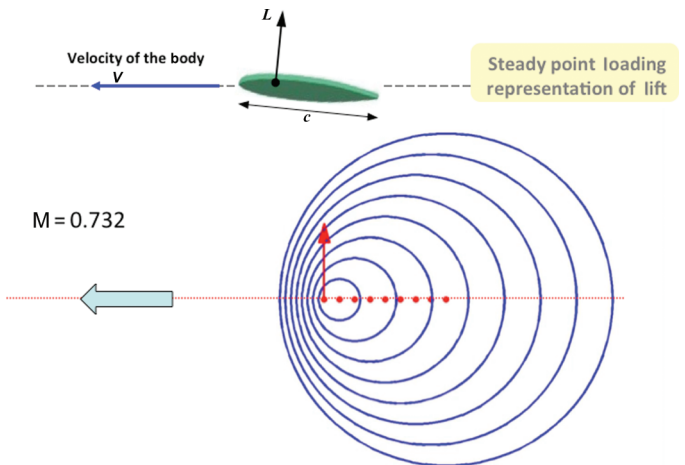


Fig. 16. Cross-sectional view of three-dimensional acoustic wavelets emitted from a constant velocity moving point source.

is the well-known Doppler effect for a stationary observer and a moving source. It is observed in every-day life when you hear a train's whistle approach you and notice that the sound changes from a high frequency to a lower frequency as the train passes by. Correspondingly, the amplitude of the oscillating pressure increases when these waves become more closely spaced and decrease when the waves are further apart. The local Mach number of the source (the ratio of the source speed to the speed of sound) controls the amplitude and frequency of these waves.

Now consider a similar subsonic moving source that is made to move in a constant radius circle, for example, at the tip of a rotor. Once again, at fixed spatial positions in close proximity to the moving source, an unsteady disturbance field is created in the stationary medium. At equal time intervals, the moving noise source initiates a sequence of disturbances that act along the circumference of the circle in the direction of the moving source. As in the case of the stationary source, each wavelet obeys the fixed space wave equation but radiates from different positions along the source trajectory. As seen in Fig. 17, the rotating geometry of the rotor problem dramatically changes the radiation pattern formed by

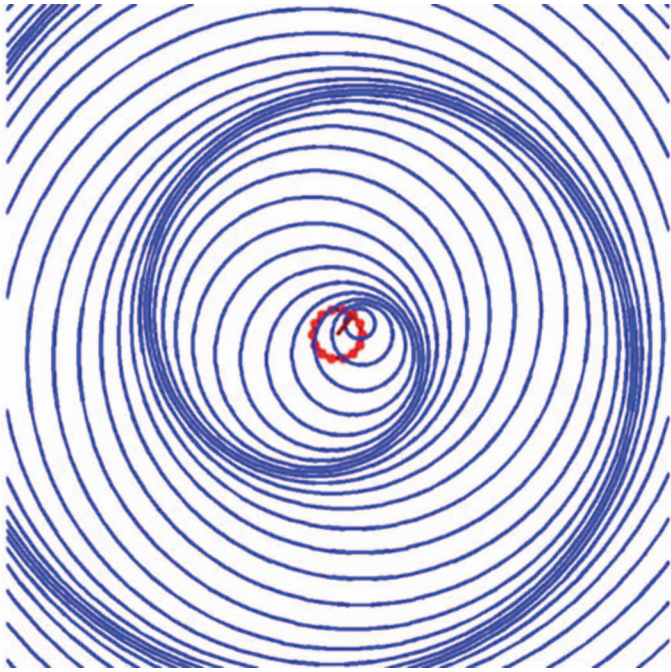


Fig. 17. In-plane cross-sectional view of three-dimensional acoustic wavelets emitted from a rotating point source pulse train.

the wavelets. Because of the rotor blade motion through the stationary medium, the outgoing waves bunch together in the medium when the source is moving toward the observer and spread apart when the source is moving away from the observer. The overall pattern repeats every complete rotor revolution.

The local Mach number of the source with respect to the medium controls the bunching of wavelets and thus the strength and frequency of the sound for the hovering rotor. For the sketch shown in Fig. 17, the local Mach number has been chosen to be the hovering tip Mach number of the UH-1H helicopter, $M_{\text{Hover}} = 0.732$. The pattern is typical for hovering helicopters and static propellers.

In forward flight, a sound source at the tip of the rotor moves in an epicycloid like pattern. As in the previous two cases, at fixed spatial positions in close proximity to the moving source, an unsteady disturbance field is created in the stationary medium. As seen in Fig. 18, the forward flight geometry further changes the hovering radiation pattern formed by the wavelets (Ref. 10). An observer ahead of the moving helicopter sees a greater bunching of wavelets, compared to the hovering case. On the other hand, an observer behind the helicopter notices a further stretching-out of the wavelets. Once again, the overall pattern repeats every complete rotor revolution. For the case shown in Fig. 18, the hover tip Mach number of the helicopter is the same as in Fig. 17. However, the helicopter is now moving forward at about 110 kt resulting in an advancing tip Mach number of 0.92, very close to the speed of sound.

These simple wave pattern arguments predict the qualitative observations of the measured data (Figs. 6–9) quite well. On the advancing side of the rotor disk, wavelets are deposited in space at close intervals because the acoustic source is moving at high speeds relative to the medium. As the wavelets propagate outward, to an observer fixed in space to a position ahead of the rotor in the direction of forward flight, these wavelets maintain their closeness. This pattern causes an increase in frequency and amplitude, as seen by the observer at this position. At an observer position behind the helicopter, these waves become weaker and larger in width. The increase in acoustic amplitude pulse in the direction of forward flight confirms is very consistent with experimental measurements.

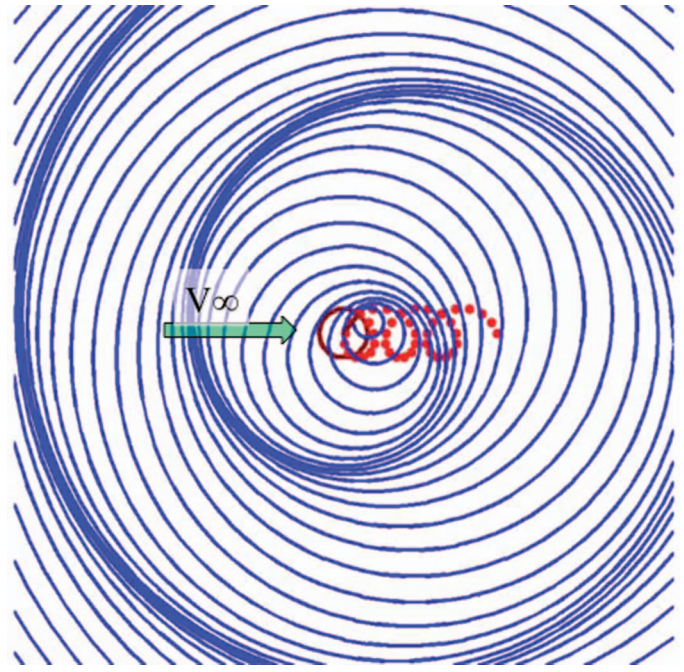


Fig. 18. Sectional view of three-dimensional acoustic wavelets emitted from a rotating and translating point source pulse train, $M_{\text{AT}} = 0.924$.

Simple wave theory also illustrates that HSI noise reduces markedly to either side of the helicopter—again predicting the trends of the in-flight experimental measurements.

Fixed space or moving coordinate system

As discussed earlier, when impulsive noise exists on a helicopter, it is likely to be the most annoying and noticeable feature of the noise signature. As we have seen, the basic kinematics of the rotating helicopter blades in translational flight tend to amplify small disturbances (wavelets) causing a “bunching of acoustic disturbances” that send acoustic energy off as directional acoustic waves. To obtain an acoustic pressure at a stationary observer position, linear acoustic analysis formally adds all of these disturbances—keeping track of the time they were emitted and the time they arrive at the observer, and adjusting for spherical spreading from their point of origin. In effect, these disturbances can be thought of as being distributed over the plane swept out by the rotor disk as it translates through the air. In hover, this plane reduces to a disk plane parallel to and infinitely close to the rotor plane as illustrated in Fig. 19. In effect, the rotor blade “turns on” these stationary point sources as the rotor blade passes over the points in space. We can use the outgoing wave “fixed space” solution to the governing linear wave equation to arrive at expressions that predict the radiated impulsive noise levels (Ref. 4). If the disturbance does not act at a point (is noncompact) as is the case for finite rotor blades, the blade chord and blade span can be divided into blade panels and the waves for each panel are calculated independently. Because the governing wave equation is linear, the noise radiated from the rotor at the observer position is the summation of these discrete panels. The noise emitted near the tip of the rotor dominates the radiating wave’s shape and amplitude.

Many early propeller noise researchers successively took this fixed space reference frame approach (Refs. 22, 23). Lower frequency propeller harmonic noise was predicted quite well. Wright extended this approach for nonaxial flight of rotors and helicopters with some success

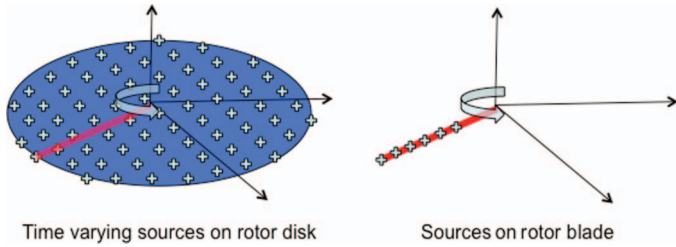


Fig. 19. Rotor blade acoustic boundary conditions for fixed-space wave equation solution: stationary and moving sources.

(Ref. 4). While the fixed space summing process can be made rigorous, mathematically deriving the source strengths that are in effect the boundary conditions to the outgoing waves can be difficult. In addition, if any point on the rotor is moving through the medium at the speed of sound ($M = 1.0$), the radiating waves emitted by each rotor panel bunch together in the extreme causing the local blade aerodynamics to change and become nonlinear. The use of linear acoustic theory for high Mach number sources becomes questionable. However, because linear theory captures many of the basic kinematics of how the fixed space sources sum to form impulsive-like waves and linear theory is valid at lower subsonic tip Mach numbers, its use is helpful in helping understand the physical origins of helicopter noise.

The parameters that govern the general shape of the impulsive noise time history are more easily seen by transforming the fixed space solution of the wave equation to a coordinate system that is attached to the moving body, in this case, the rotor blade. A sketch of this problem formulation is given in the right half of Fig. 19. Lowson and Ollerhead (Ref. 3) developed this kind of approach for moving point forces (a point force that acts on the center of a panel) and applied this approach to the helicopter harmonic noise radiation problem. They achieved results similar to those of Wright, which were somewhat successful in predicting lower frequency harmonic noise but could not capture the nonlinear behavior of the noise.

A moving coordinate system approach, for bodies in arbitrary motion, was rigorously developed by Ffowcs Williams and Hawkings (Ref. 24). The authors used generalized functions to develop an inhomogeneous acoustic governing equation. Although the mathematics to do this transformation are complex and require the use of “generalized functions,” the actual calculations used to compute the noise are simpler because of the incorporation of the boundary conditions on the moving blade directly in the integral equation solution. Farrasat, using generalized functions, developed many useful forms of this equation for rotorcraft and propeller noise applications (Refs. 25 and 26). Brentner has developed computer programs that are based on these formulations to numerically predict rotorcraft harmonic noise radiation (Ref. 27). One form of the solution for a stationary observer is (Eq. (3))

$$\begin{aligned} p'(\vec{x}, t) = & \frac{\partial}{\partial t} \iint \left[\frac{\rho_0 v_n}{r |1 - M_r|} \right]_{\tau} dS(\vec{\eta}) - \frac{\partial}{\partial x_i} \iint \left[\frac{\rho_{ij} n_j}{r |1 - M_r|} \right]_{\tau} dS(\vec{\eta}) \\ & \text{Monopole} \quad \text{Dipole} \\ & + \frac{\partial^2}{\partial x_i \partial x_j} \iiint_V \left[\frac{T_{ij}}{r |1 - M_r|} \right]_{\tau} dV(\vec{\eta}) \quad (3) \\ & \text{Quadrupole} \end{aligned}$$

and

$$T_{ij} = \rho u_i u_j + P_{ij} - a_o^2 \rho' \delta_{ij}$$

where η is the axis of the coordinate system attached to the moving blade, dS is the elemental area of the blade, ρ_0 is the undisturbed density of

the air, v_n is the normal velocity produced by the body (airfoil), $\rho_0 v_n$ represents the disturbances due to blade thickness, $p_{ij} n_j$ is pressure normal to the surface of the area.

The integral solution to the governing inhomogeneous linear wave equation, in this general form for rotors, requires some special interpretations. There are three acoustic source terms: a monopole term and a dipole term that are integrated over the surface of the blade and a quadrupole term that is integrated over all space that can contain contributions to the acoustic pressure. All the terms require that the computations be performed at the correct retarded time as depicted by the “square parentheses”—so that the acoustic perturbations caused by the rotor blade at time, τ , arrive at the correct observer time, t . The expression relating these times is

$$t = \tau + \frac{r}{a_0} \quad (4)$$

where r is the distance from the observer to the source at the emission time.

It should also be noticed that the factor $1/|1 - M_r|$ appears in all three terms and comes about because of the motion of the source. The source Mach number in the direction of the observer, M_r , controls the strength of this factor. At large M_r below Mach numbers of 1, $|1 - M_r|$ becomes small and $1/|1 - M_r|$ becomes large. This increase in level is depicted in the wavelength sketches of Figs. 16–18 by the close spacing of the wavelets. When the Mach number of the source (wavelet) approaches one, the integrand of these integrals become singular, causing local radiated waves to accumulate and increase in amplitude. When this happens, nonlinear aerodynamic effects become quite important. They directly influence the acoustic solution through the quadrupole term and indirectly through the dipole term, changing the force magnitude and local distribution on the body. The author first realized the importance of nonlinear aerodynamics for accurate prediction of rotor acoustics after many experimental observations and many efforts to match linear theory with data (Ref. 28). Major improvements in correlation of theory with data were achieved once the transonic the nonlinear aerodynamics of the rotor were accurately captured in the problem formulation.

Thickness noise

Near the tip-path plane of the rotor, the acoustic signal in Figs. 6–9, was seen to have a distinct, almost symmetric, large negative pressure pulse that radiates in the direction of forward flight. For helicopters flying with advancing tip Mach numbers in the 0.75–0.85 range, the shape of this pulse can be explained by considering the first term of Eq. (3) and ignoring the other two terms (Ref. 28). The numerator of the integrand of this first term is $\rho_0 v_n$. It describes the mass of fluid per area that is displaced by the blade at a position in space as it moves through the air. Since density is assumed constant for the small perturbations, this variation in mass is proportional to the velocity normal to the mean chord of the rotor blade, integrated over that elemental section of the blade as sketched in Fig. 20. The thickness noise model of the rotor blade can be thought of a series of “positive” sources to separate the air followed by a series of negative sources (“sinks”) to return the flow to its free-stream direction and essentially “close” the airfoil. Similar arguments are used in classical thin airfoil theory.

To illustrate the formation of thickness noise pulse in a simple way, we will represent this chordwise distribution of sources and sinks at any station along the blade chord by one source and one sink of equal strength—chosen to represent the maximum thickness of the airfoil and located at the one-fourth chord line and the three-fourth chord line, respectively. In effect, we now have represented the thickness of the blade by a radial distribution of equivalent bodies of revolution (bottom

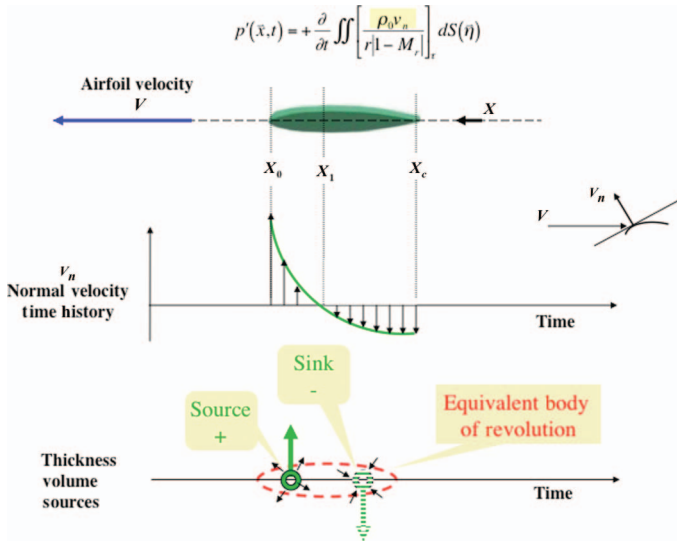


Fig. 20. Thickness noise modeling.

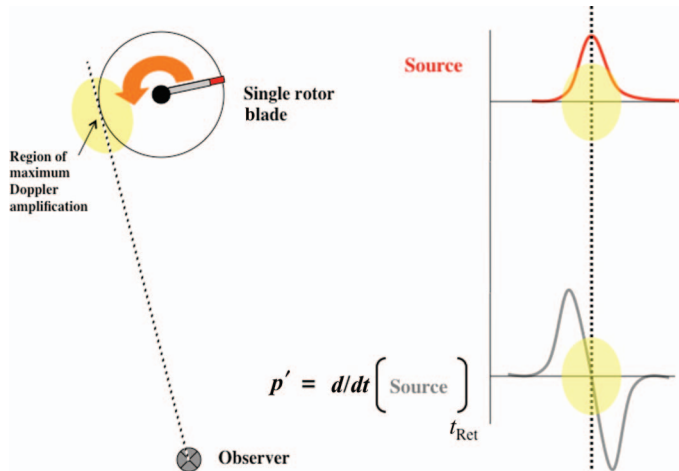


Fig. 21. Graphical description of a rotating “source” thickness noise pulse shape.

sketch in Fig. 20). The source and sink strengths at any spanwise station have been chosen so that the air flows around the blade are similar to an airfoil of the same overall thickness; that is, there is no flow through the surface of the blade. For simplicity in explanation, we will also only consider the disturbance from the outer 10% of the blade and restrict these initial arguments to hover.

A top view sketch of the geometry of this simplified problem is given on the left side of Fig. 21 for a single-bladed helicopter rotor. The corresponding values for the single source strength, as measured at the observer position, are shown in the upper right of the same figure. The derivative of this source at the observer location is the acoustic pressure and is shown in the lower right-hand side of the same figure. The dashed line and highlighted area locates the time when the source, emitted at τ , is moving directly toward the observer, that is when M_r is a maximum. As seen from this figure, the acoustic time history is a positive-negative pulse—unlike the measured flight data that were attributed to thickness noise.

Figure 22 is a sketch of the noise generation process for a “sink” (negative source). The summing process is the same as for the source

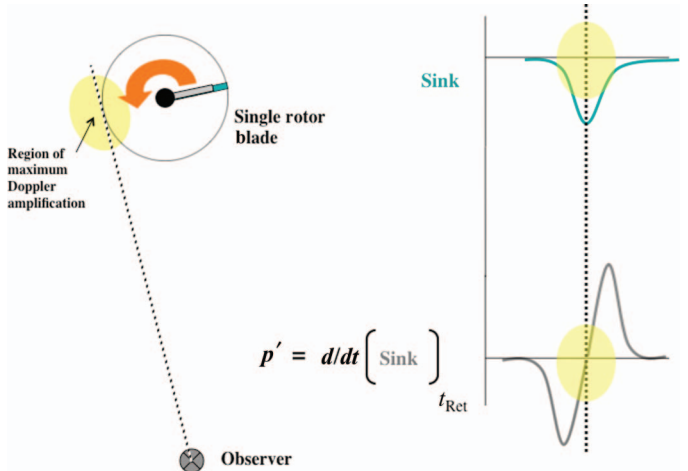


Fig. 22. Graphical description of a rotating “sink” thickness noise pulse shape.

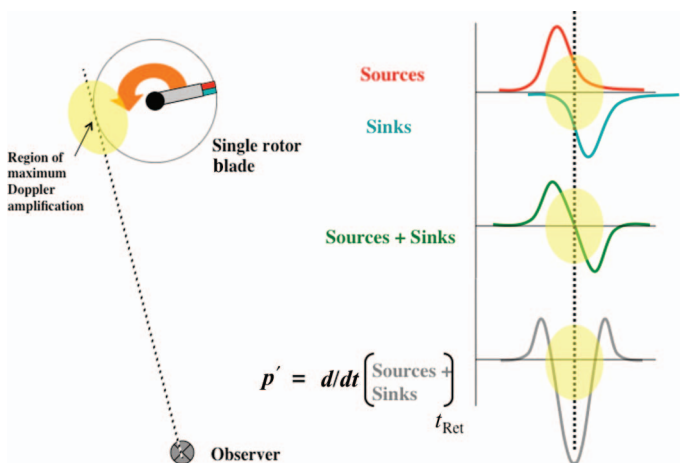


Fig. 23. Graphical description of a rotating “source-sink pair” thickness noise pulse shape.

and yields a similar shaped pressure time history at the observer, but with a reversed sign. It also does not match the pulse shape of the measured data.

As discussed earlier, the thickness boundary condition has generated a source and sink pair that rotates with the rotor at a fixed distance apart along the chord of the airfoil. At a fixed position in space on the rotor disk, the “sink” pressure perturbation is delayed in time from the “source” pressure perturbation. Although the “source” and “sink” waveforms are identical, they are of opposite sign. When the time histories are added together at the observer time, the delay causes a nonzero pressure perturbation time history at the observer. The time derivative of this perturbation time history is the radiated noise measured by the observer. This calculation process is graphically depicted in Fig. 23 and is the physical mechanism that produces the thickness noise pulse shape. As shown in Fig. 23, the resulting pulse time history is symmetrical and is characterized by a large negative pulse preceded and followed by smaller positive pressures. Although not illustrated here, these same arguments yield similar symmetrical negative pulse shapes for a helicopter in forward flight at low-to-moderate advance ratios.

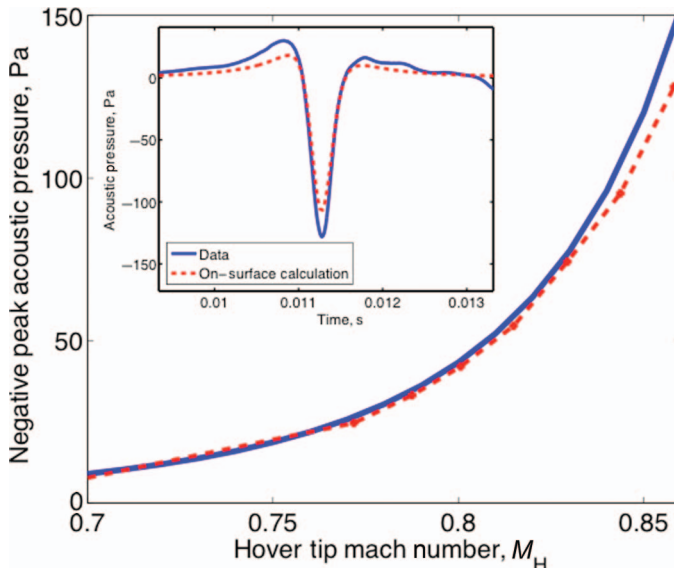


Fig. 24. Theory/experimental hover comparison of thickness noise at low Mach numbers.

When compared to the measured data in Figs. 6–9, this simple source-sink singularity model of “thickness noise” captures the negative pulse shape characteristics quite well at low-to-medium advance ratios and advancing-tip Mach numbers.

When rotor blade thickness is represented by many “sources” and “sinks” distributed along the blade chord and span, this same general pulse shape prevails as shown in the insert on Fig. 24 for a hover tip Mach number of 0.85. This figure also compares thickness noise theory with some in-plane acoustic measurements made in the University of Maryland Acoustic Hover Facility. The AH-1 1/7th-scale untwisted model rotor was run at very low angles of attack to minimize hover flow recirculation effects. The data were also averaged in time to pull out the

periodic character of steady thickness and loading harmonic noise. Good comparison between thickness noise theory and measurement is shown at these low hover-tip Mach numbers (Ref. 28).

High-speed impulsive noise

An early comparison (~1978) between thickness noise theory and experiment is shown in Fig. 25 for the UH-1 helicopter in forward flight at higher tip Mach numbers. The experimental acoustic data were taken using the formation flying measurement technique on two separate test programs (Ref. 29). Fair comparison between thickness noise theory and experiment in terms of pulse amplitude is shown at lower advancing tip Mach numbers, with theory generally underpredicting the peak amplitudes of the negative pulse. The pulse shapes are quite similar to those predicted and measured in forward flight. However, as the advancing-tip Mach number increases, major discrepancies between theory and experiment are noted. At an advancing tip Mach number of 0.918 (Fig. 25), the measurements indicate that a major change in the pulse shape has taken place. The negative pulse at lower advancing tip Mach numbers has dramatically increased in amplitude and changed into a “saw-toothed” wave. The radiated noise has totally changed character; going from a soft sounding series of impulses to a harsh cracking impulsive sound with a sharp increase in peak level. At these high tip Mach numbers, a pressure discontinuity (shock wave) was measured by the far-field microphone. It is clear that the rotor acoustic problem is no longer governed entirely by linear acoustics.

Upon identification of this phenomenon, an acoustics wind tunnel test on a Mach-scaled UH-1H was performed in the Army 7 × 10-ft wind tunnel at NASA Ames (Ref. 10). To avoid reflections from the wind tunnel walls, a 4-inch “Scottfelt” foam liner was installed in the closed section tunnel as shown in Fig. 26. Near in-plane microphones were placed as close as possible to those microphone directivity angles that were measured at full-scale, in flight. When the scaled experimental wind tunnel noise measurements were compared with those taken at the same nondimensional distances and angles to those taken in flight, good agreement in pulse shape and amplitude was demonstrated

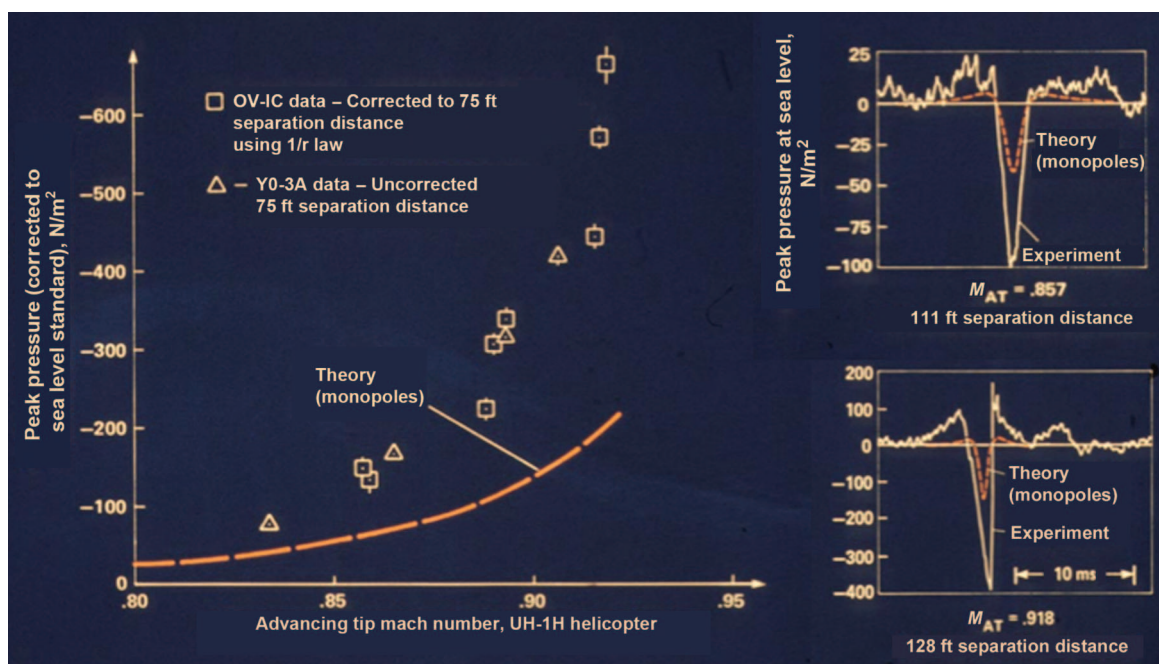


Fig. 25. Theory/experimental comparison of in-plane harmonic noise at high advancing tip-Mach numbers.

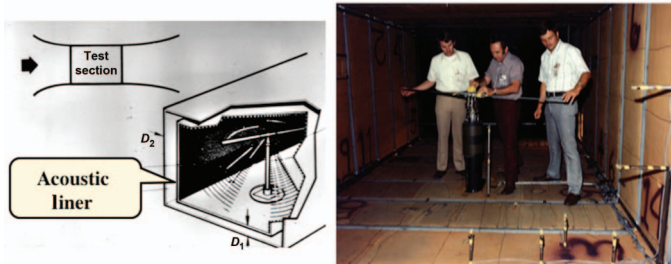


Fig. 26. Acoustic measurements of a scaled UH-1H model rotor in the Ames 7 x 10-ft Wind Tunnel.

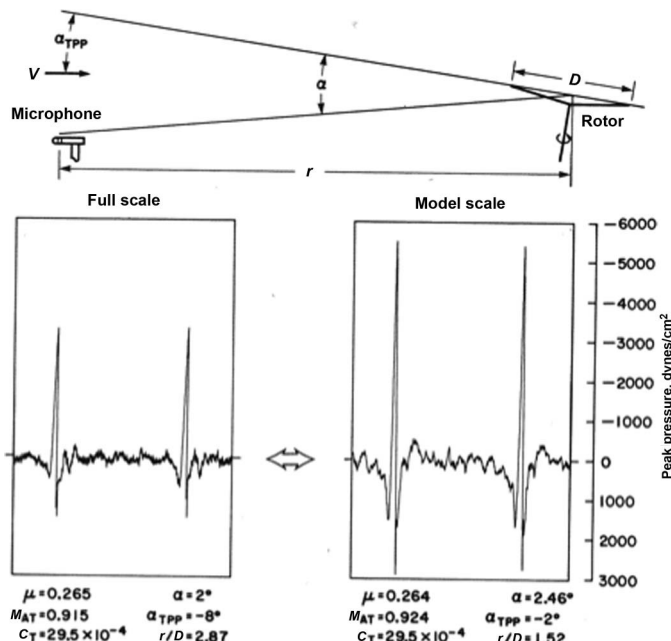


Fig. 27. Comparison between 7 x 10-ft wind tunnel and in-flight acoustic data.

(Fig. 27). (Note that the nondimensional distance from the rotor hub to the microphone for the wind tunnel and flight is different in Fig. 27.)

This scaled rotor model tunnel test demonstrated that the major features of thickness noise could be quantitatively reproduced in model scale—especially the transition of the thickness noise from a symmetrical pulse shape to one that was more saw-toothed in character. At high advancing tip Mach numbers, the saw-toothed wave dominated the acoustic radiation and was, in fact, a low level shock wave that was radiated to the acoustic far field. It is interesting to note that the then current theoretical acoustic models of the time attributed this change in shape and in level to the rapid change in drag on the advancing side of the rotor. While the drag does change because of transonic effects, it is not a primary cause of the increasing acoustic levels or pulse shape changes that were measured. Nonlinear aerodynamic effects needed to be included in the basic acoustic modeling to capture the physics of the HSI noise problem. A theoretical formulation of the problem that included these governing effects had not yet been developed.

Schlieren photographs (Refs. 10, 29) reinforced the observation that the physics of the HSI problem were dominated by tip Mach number. The 1/7-scale model wind tunnel measurements also revealed that the thrust of the rotor did not substantially affect the level or shape of the HSI noise radiation. These factors led to the decision to perform a more detailed experimental exploration, using a 1/7th-scale model of the UH-

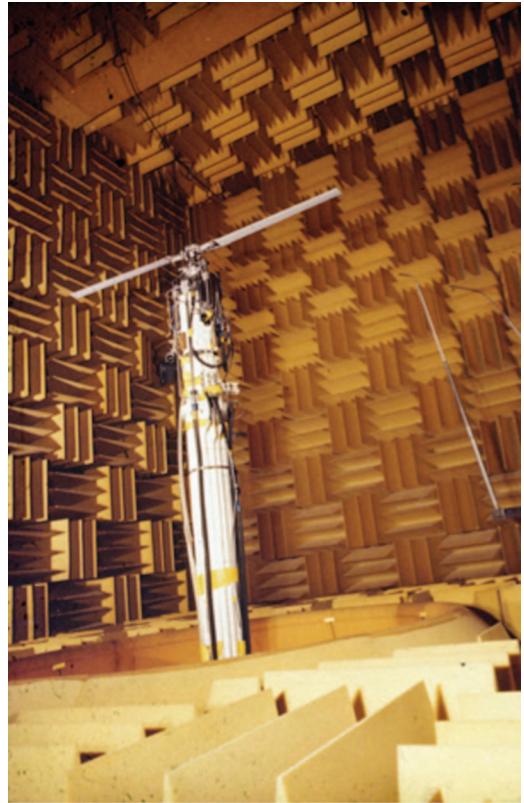


Fig. 28. High-speed hover rotor testing in Army Anechoic Test Facility.

1 rotor, of HSI noise in hover, at low nominal thrust settings in a specially designed anechoic hover chamber (Fig. 28). Twisted and untwisted UH-1 geometrically scaled rotors were run at several hover tip Mach numbers similar to the advancing tip Mach numbers that were run for forward flight testing. Because safety was also easier to maintain in these hover conditions, very high tip Mach numbers could also be explored.

The hovering acoustic results are shown in Figs. 29 and 30 for an in-plane microphone at 1.5 diameters from the rotor hub (Ref. 30). As in forward flight, a dramatic change in pulse shape is observed for small changes in tip Mach numbers. The peak noise level almost doubles, and the waveform becomes saw-tooth in character—with a shock wave defining the near vertical rise in acoustic pressure. Over this small hover tip Mach number range, the waveform has transitioned (delocalized) from a nearly symmetrical shape to a saw-toothed shape—showing that a shock wave on the rotor is propagating to the far field in this steady hovering condition. It is this large amplitude saw toothed wave that has characterized the acoustic radiation of the UH-1H helicopter on cold days. In high-speed flight, ground observers on the order of 10 miles away can hear this HSI noise, before the helicopter overflies an observer.

The idea that a hovering rotor operating at high subsonic tip Mach numbers could radiate shock waves was somewhat controversial at the time of these fundamental experiments (Ref. 31). To be sure that these physics were being modeled correctly, some early computational fluid dynamics (CFD) computations were made by several authors and validated by measuring the regions in the flow where the aerodynamic flow field became supersonic (Fig. 31). Further detailed comparison of the CFD results with experimental measurements (Fig. 32), confirmed that when the flow field “delocalized,” shock waves on the surface of the rotor were connected to the acoustic far field and were responsible for the pulse shape change recorded on the microphones (Ref. 31).

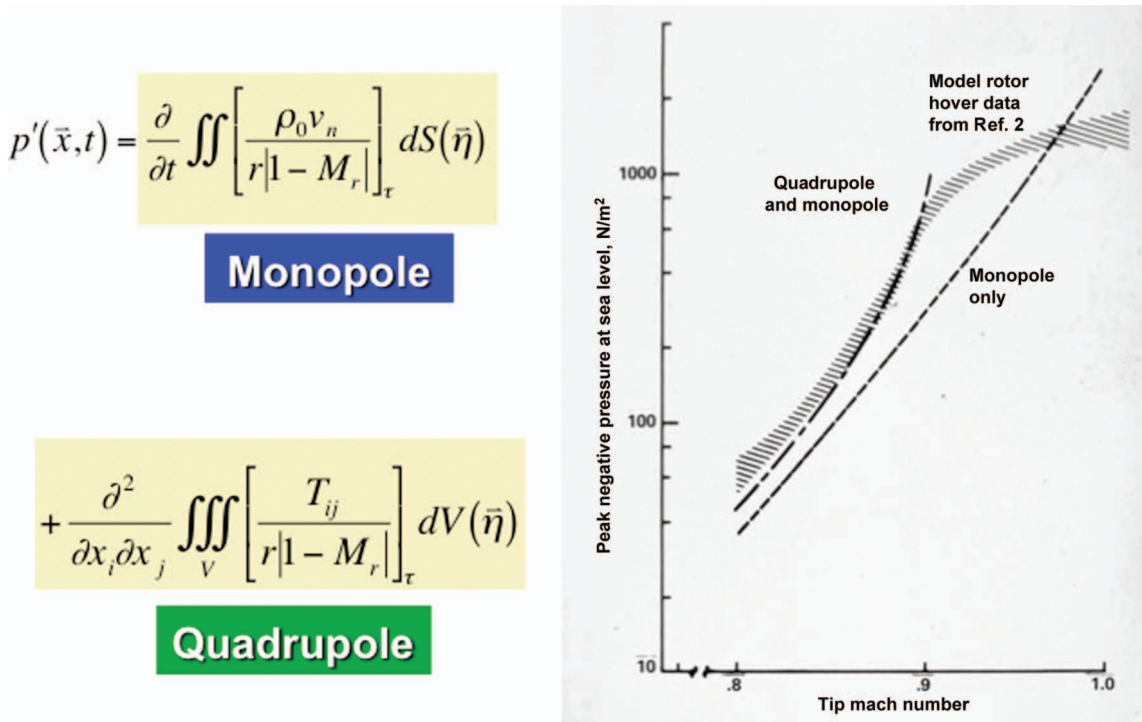
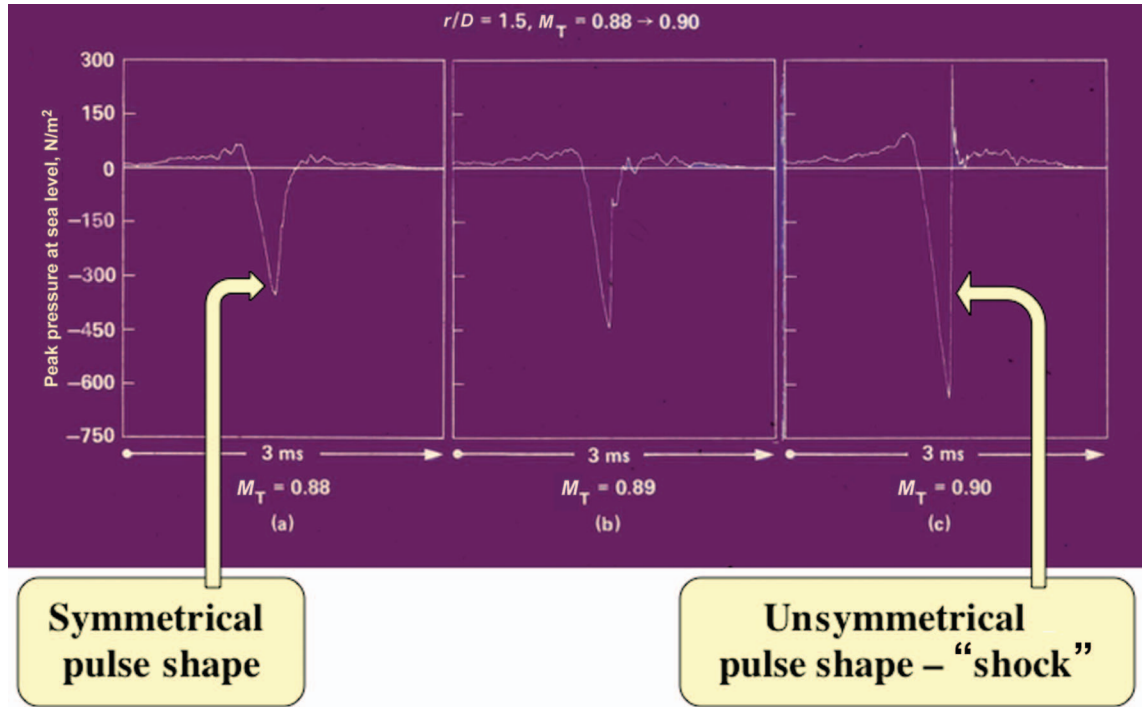
Fig. 29. The measured transition of in-plane thickness noise to HSI noise, $r/D = 1.5$.

Fig. 30. Rotor acoustic delocalization in hover.

Three-dimensional constructions of the flow field using holograph tomography confirmed the existence of a rotating shock structure that was attached to the rotor and extended to the measurement microphone (Ref. 32).

The measured peak negative pressures of this nonlifting, hovering rotor are shown in Fig. 29 as a function of hover tip Mach number, from $M = 0.8$ to 1.0. Also plotted on this figure are the predictions of noise

using the first term of Eq. (3) (monopole sources). It is clear that linear theory underpredicts the peak levels over most of Mach number range shown—but becomes closer to the measured data at lower tip Mach numbers. Including nonlinear effects by calculating the third term of Eq. (3) (quadrupole sources) makes the agreement better at low tip Mach numbers and describes the beginning of the pulse shape changes due to delocalization (Ref. 33). However, for hover, with the rotor operating at

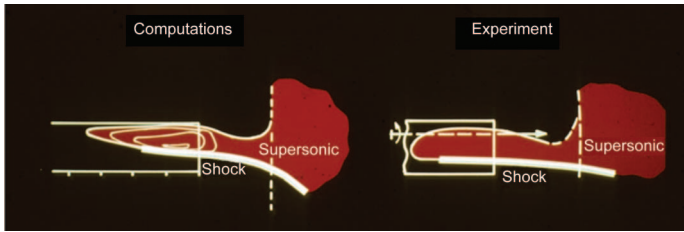


Fig. 31. CFD (ROT22) and measurements (Ref. 33) of acoustic delocalization.

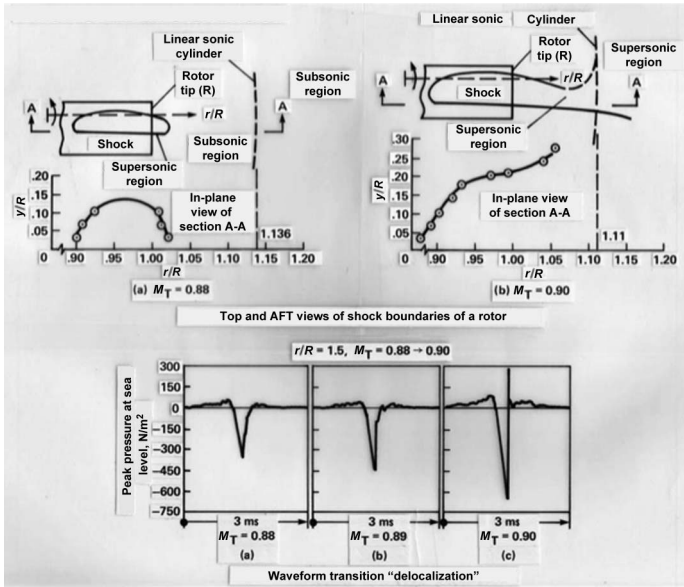


Fig. 32. Measurements and CFD predictions of the acoustic delocalization process.

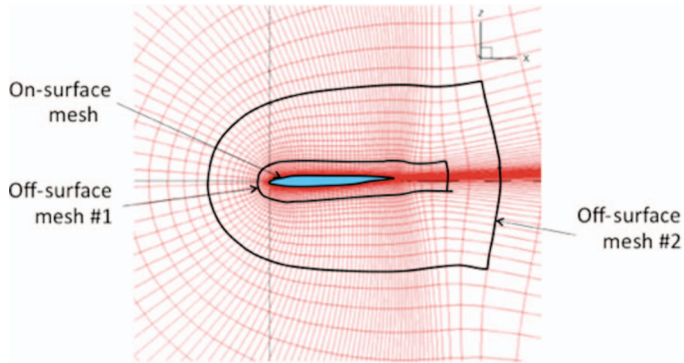


Fig. 33. A sketch of on-surface and off-surface control surfaces for CFD-based computations (circa 2009).

high tip Mach numbers beyond delocalization, calculating the nonlinear aerodynamic contributions by using quadrupoles, becomes difficult and error prone. Instead, as depicted in Fig. 33, today CFD is used to predict the aerodynamic field surrounding the rotor (Refs. 34, 35) and control surfaces that capture acoustic waves at those surfaces are used in a linear solution to the wave equation to accurately predict thickness and HSI noise levels in the acoustic far field. This will be discussed in more detail later in the paper.

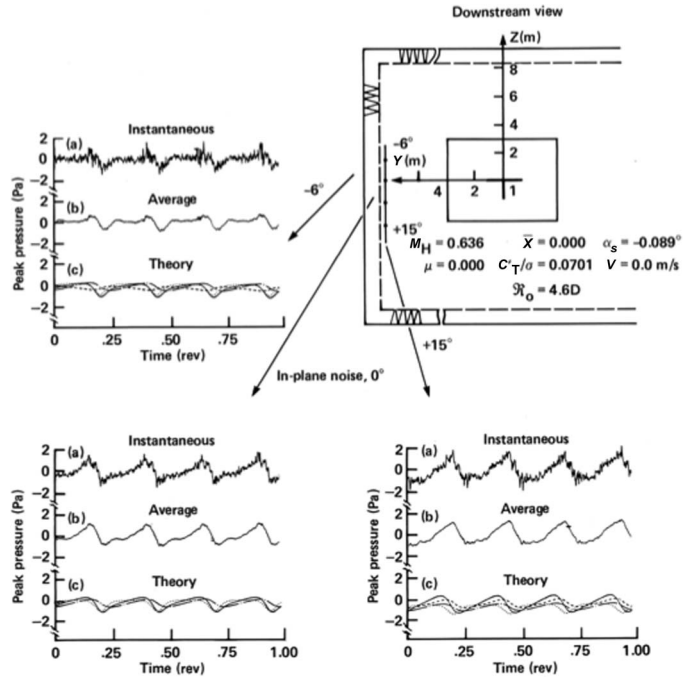


Fig. 34. Low-frequency noise of a hovering model rotor in the DNW: Theory/experiment.

Loading noise

The lift and drag of the rotor blades also contribute to the radiated noise through the second term of Eq. (3). The rotating dipoles create time histories, at a far-field observer, that are dependent on the time histories of the lift and drag of the rotor. For a propeller or a rotor in axial flight, the thrust and drag are usually fairly constant with azimuth. For equally spaced blades, the radiating noise becomes harmonic repeating at rotational frequency times the number of blades. At low tip Mach numbers, the noise is usually of low frequency in nature. Because the loading is the same at any azimuth angle, the radiation pattern is symmetrical with azimuth.

However, for a helicopter in nonaxial flight, the loading noise varies markedly with azimuth position and the radiation pattern with azimuth also changes. In addition, the noise also changes with the tip-path-plane angle, depending on the relative strength of the lift and drag vector dipoles. The dipole computation procedure is quite similar to the thickness calculations (Ref. 29). For observer positions below the thrusting rotor plane, the net result is a plus-minus pulse shape that depends strongly of the relative magnitude and the time history of the thrust and drag of the rotor at each radial station along the blade. This shape is shown in Fig. 34 for a hovering four-bladed model-scale rotor tested in the near anechoic part of the Duits-Nederlandse Windtunnel (DNW) (Ref. 36).

It is apparent that dipole noise and thickness noise both contribute to the radiated noise time history. The sum of the monopoles and dipoles (first and second terms of Eq. (3)) determines the time history pattern that is measured in the acoustic far field. Because the factors multiplying each term are different, their relative strengths are different. For the relatively high advancing tip Mach numbers of conventional rotors ($M_t \geq 0.85$), thickness noise dominates the far-field radiation. However, as the advancing tip Mach number of the rotor is lowered, the second “dipole” term of Eq. (3) becomes more dominant.

The high advancing tip Mach numbers of the Vietnam era helicopters caused many of the delocalized phenomenon described as HSI noise.

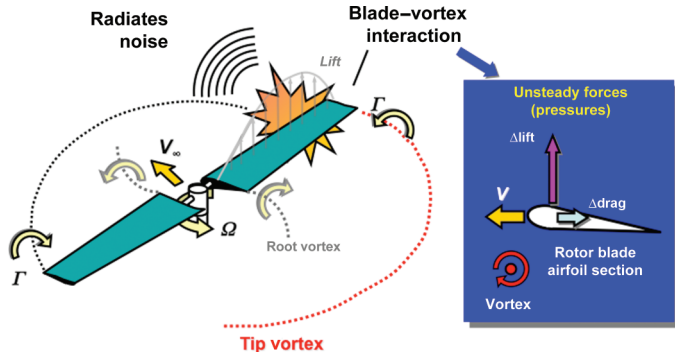


Fig. 35. Physical mechanisms of BVI noise.

Helicopter designs favored maximizing lift in hover and consequently resulted in high hovering tip Mach numbers. When flown in forward flight, the resulting advancing tip Mach number of the rotors became very high, resulting in very high levels of impulsive noise. The high advancing tip Mach numbers of these helicopters also limited their forward flight aerodynamic performance.

The lower hover tip Mach numbers of many of today's helicopter has allowed the cruising speeds to be increased while holding the advancing tip Mach number below supersonic speeds. This also results in larger advance ratios with larger retreating blade stall regions—forcing the rotor to produce larger unsteady forces to balance increases in rolling moment. These design changes also change the relationship between the loading and the thickness contributions to the radiating noise—with unsteady loading noise growing more important at these higher advance ratio/lower hover tip Mach number conditions.

Increasing advances in electric motor technology have encouraged the development of the electrically powered helicopter. Higher torque at lower rotational speeds has favored operation at low tip speeds. At these low tip speeds, harmonic noise is dominated by dipole noise sources.

Blade–vortex interaction noise

As discussed earlier, BVI impulsive noise occurs when the rotor operates near its own shed wake. The tip vortices trailed behind each rotor blade interact with the following blades creating sharp changes in blade pressure and thus local lift changes. The pressure changes create local unsteady forces on the fluid that sum at a far field observer and cause BVI noise. The basic aerodynamics of BVI is depicted in Fig. 35 for a partial revolution of a two-bladed main rotor system. The trailed vortex from each blade induces a rapid change in blade angle of attack, which cause a change in blade pressure (in the lift and drag directions). The changes in lift are normally about an order of magnitude larger than the changes in drag—causing the largest BVI noise radiation to be radiated out of the plane of the rotor's tip-path plane. A sketch of a typical in-flight measurement of BVI noise is shown in Fig. 36 for a microphone located about 30° below the plane of the rotor (Ref. 12). A rapid series of positive pressure pulses are seen to occur just before each thickness noise pulse. A series of smaller pulses of negative sign that occur more frequently is also observed in these measurements. These pulses are due to tail rotor thickness noise. Because the BVI pressure pulses and tail rotor harmonic noise are narrow in width, they radiate most, but not all, of their energy in the mid-to-high-frequency range and can easily annoy a far-field observer.

The key governing parameters of BVI noise radiation are advance ratio, the trace tip Mach number of the BVI interaction, the separation distance between the rotor's tip-path plane and the previously shed tip

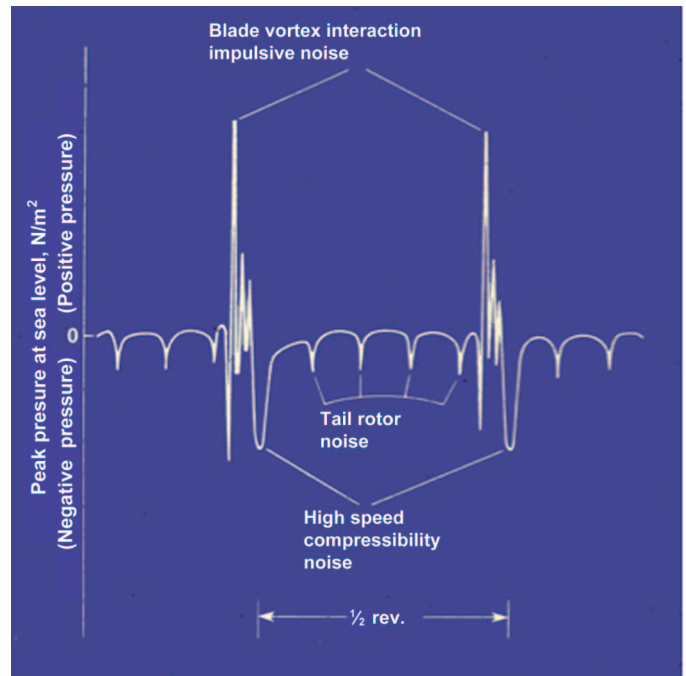


Fig. 36. Sketch of BVI noise, 30° down microphone position.

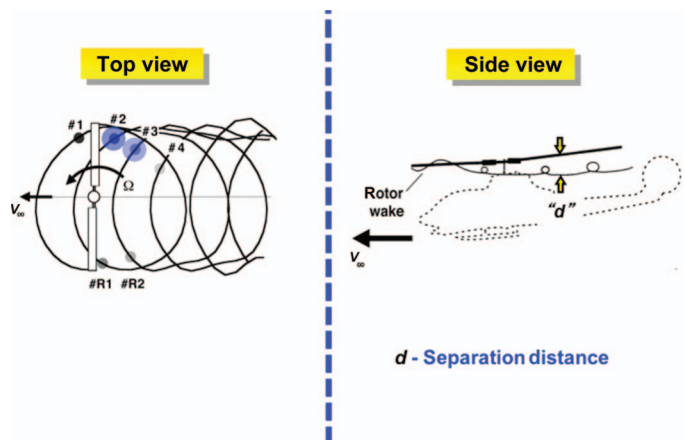


Fig. 37. Interaction geometry of BVI noise for a two-bladed rotor.

vortices, and the strength of the shed vortex from each blade (Refs. 13 and 18). A top and side view of a two-bladed helicopter main rotor undergoing BVI is sketched in Fig. 37. The timing of the wavelet summation process is a strong function of the geometry of the interaction and the hovering tip Mach number of the rotor. The BVI geometry is controlled by advance ratio; the ratio of the helicopter's forward velocity to its hovering tip speed (Refs. 2,12). For the two-bladed rotor shown, four advancing side interactions (#1–#4) and two retreating side interactions (#R1 and #R2) are shown on the left side of Fig. 37. The right side of this figure shows a two-dimensional sketch of the side view of the helicopter and its generalized wake. Under most level flight conditions, the rotor's shed tip vortices pass under the rotor at some aggregate distance d . The tip-path-plane tilt with respect to the velocity vector and the average induced velocity of the rotor control the separation distance, whereas the average induced velocity is a function of the rotor's thrust coefficient. The thrust coefficient also controls the strength of the shed vortices.

The BVI wavelet summation process for a two-bladed rotor is depicted in Fig. 38. A good way to visualize the acoustic summing process

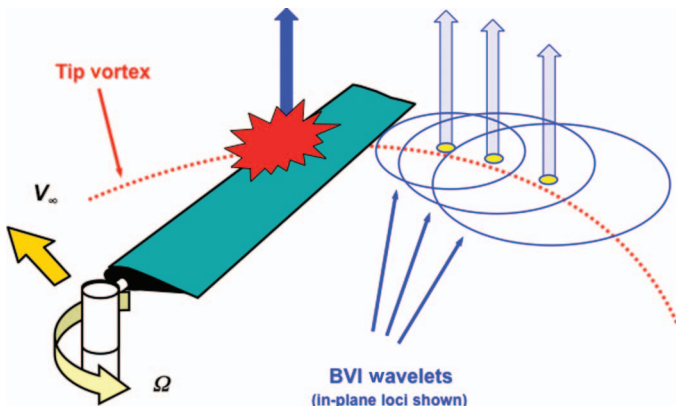


Fig. 38. Sketch of the BVI wavelet summation process.

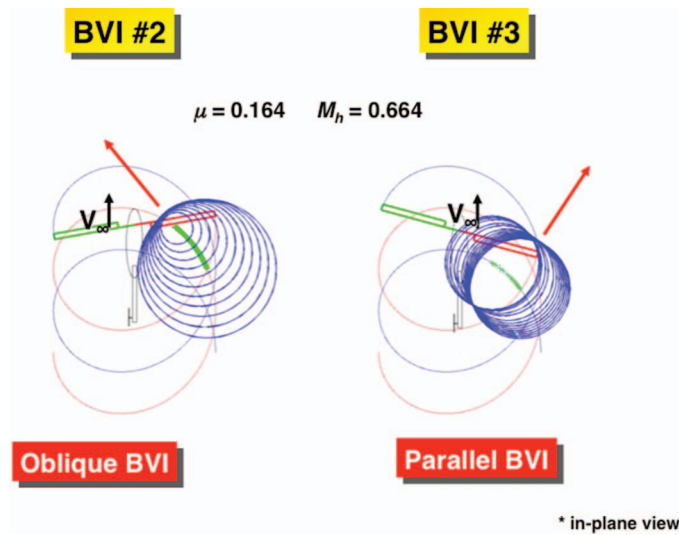


Fig. 39. Formation and directivity of BVI waves.

is to think of the blade as being made up of a series of spanwise charges (impulses) that are triggered (set off) when the blade and rotor wake interact. The charges produce wavelets that, when added together with the appropriate strengths, produce BVI noise radiation (Ref. 37). To a great extent, the Mach number of the interaction trace in the fluid determines the strength and directivity of the resulting noise radiation. Trace Mach number profiles that are near Mach 1 and those that approach infinity create bunching of waves in preferred directions.

Sketches of the wave formation process for a two-bladed helicopter, flying at an advance ratio of 0.164 with a hover tip Mach number of 0.664, are shown in Fig. 39 (Refs. 37, 38). Two interactions radiate significant BVI noise: an oblique interaction (BVI #2) and a parallel interaction (BVI #3). BVI #2 begins at the tip of the rotor blade and moves inward toward the hub triggering small acoustic wavelets. The spatial summation of these wavelets forms an acoustic wave, which radiates forward and to the port side of the helicopter, which passes through the front part of the helicopter cabin. The ratio of the speed at which these disturbances travel in the medium to the speed of sound along the trace of the interaction is called the trace Mach number and generally characterizes the directivity and radiation efficiency of each BVI. As in the case of thickness noise, Mach number plays an important role in the grouping of these wavelets. BVI #2 has a trace Mach number that begins supersonically but decelerates to subsonic speeds (left side of Fig. 39) as the interaction moves in-board along the radius. The darkness of the line

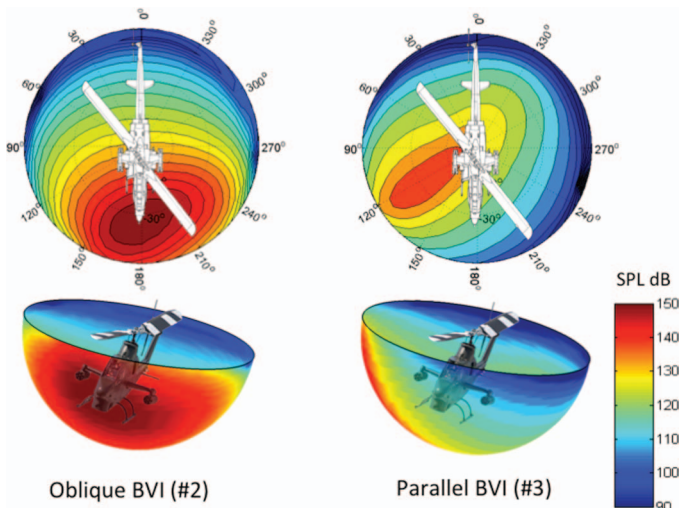


Fig. 40. Radiation spheres for BVI noise: oblique BVI #2 and parallel BVI #3.

at the observer indicates that wavelets from BVI impulses are arriving at nearly the same time, indicating that a strong acoustic wave is developing along a line almost tangent to the wake epicycloid pattern. BVI #3, a near parallel BVI with high supersonic trace Mach numbers (right side of Fig. 39), triggers all of its wavelets nearly simultaneously, sending acoustic energy forward and to the starboard side of the helicopter. A strong acoustic pulse is likely because all of the acoustic wavelets nearly add in-phase.

The calculation of the radiated noise for BVI proceeds in a similar manner to thickness noise. Use is made of the free-space outgoing solution of the governing wave equation, and wavelets are simply summed in the stationary medium to yield the radiated noise. As in the case of thickness noise, the actual calculations of BVI noise are made easier in an on-blade coordinate system. For BVI, the dominant terms of the governing Ffowcs Williams and Hawkings equation are the dipole (pressure) and quadrupole terms—the second and third terms of Eq. (3). Because the quadrupole pressure fluctuations are normally small and occur near the blade surface, the quadrupole contributions to BVI noise are also small and can be neglected. The exception is noise predictions near the plane of the rotor where disturbances may accumulate and alter the aerodynamics and resulting acoustics of BVI noise radiation.

Some calculations of BVI far-field noise directivity patterns for these two interactions are shown in Fig. 40 for a hemisphere surrounding the rotor. It is clear that the previous geometric arguments support the calculated radiation patterns. BVI #2, an oblique interaction with a trace Mach number profile that is close to 1, generally predominantly radiates energy ahead of and slightly to the right under and above the plane of the rotor. BVI #3, a near parallel interaction with a trace Mach number near infinity, radiates impulsive energy downward and upward to the right side of the rotor. The BVI strengths shown in this figure were derived using indicial aerodynamics and a prescribed wake (Refs. 39, 40) that have been validated by experiment. Please note that the predicted levels shown are for a sphere far away from the helicopter (far-field noise) with the radius of the sphere centered on the rotor hub, but projected inward and amplified using $1/R$ corrections to more clearly show directivity trends. This type of representation of noise levels has become somewhat standard throughout the industry and is often used to represent flight-test directivity measurements.

Because the details of the helicopter wake models are often lacking and difficult to measure, first principles prediction of BVI noise is not

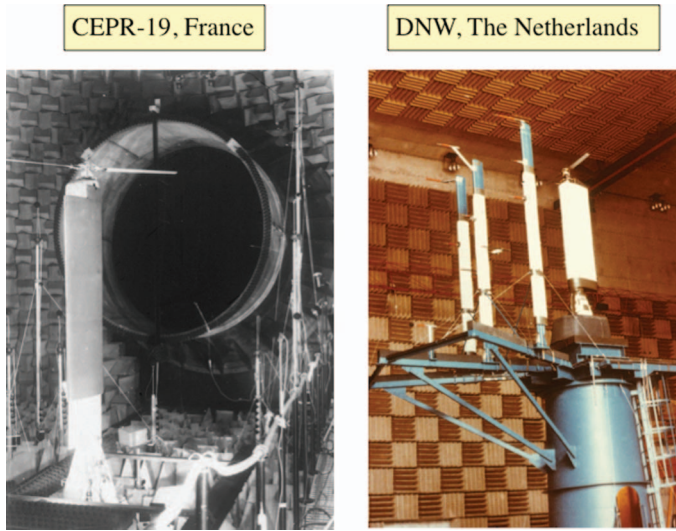


Fig. 41. Rotor testing in two open jet anechoic wind tunnels: CEPR-19 and DNW.

always reliable. To surmount this, use has been made of scaled main rotor models to estimate BVI noise radiation. The small-scale testing also allows different rotor configurations to be tested in a cost effective manner at early stages in the design process. To obtain good noise measurements, the rotor should be evaluated in an environment that does not distort the acoustic measurements. This normally requires that the rotor be tested in quiet anechoic facilities, where acoustic reflections and distortions from

near-by surfaces are minimal. Two such facilities are shown in Fig. 41: the CEPRA-19 tunnel in France and the DNW in The Netherlands.

To demonstrate that a small-scale rotor can replicate the BVI acoustics of a full-scale rotor, a model-scale AH-1 rotor was tested in both facilities in the early 1980s; becoming the first rotor acoustic test in both facilities (Ref. 41). The cooperative U.S. Army-led French and German test teams were able to show that for a limited testing envelope where BVI noise often dominated the radiated noise, model-scale rotors could replicate the details of BVI fairly well as shown in Fig. 42. For low-to-moderate advance ratios, the shape and level of the measured acoustic time histories were reproduced quite faithfully when appropriately scaled. Unfortunately, at high advance ratios, the comparisons between model and full-scale acoustic time histories deteriorated. Nevertheless, this program was followed by many scaled rotor acoustic tests and has proven to be a good way to validate theoretical prediction methods and to explore novel rotor designs.

Larger scale BVI acoustic testing has also been performed in the 40 × 80-ft tunnel at NASA Ames Research Center. The absorptive liner in the closed section tunnel was enlarged to 39 inches in the late 1990s to reduce wall reflections in the 120-Hz and above frequency range (Ref. 42). Background noise due to the operation of the tunnel drive motors was also reduced. Recent acoustic testing of larger scale rotors has been very encouraging at low advance ratios where BVI tends to be important. However, the size of the 40 × 80-ft wind tunnel section is attractive for full or large-scale testing, and consequently, is used predominantly for that purpose. The acoustic testing of large- or full-scale rotors is limited by the inability to position microphones in the acoustic far field and by the ability of the deep acoustic liner to absorb the lower frequency wall reflections. Smaller rotor testing (~10 ft in diameter)

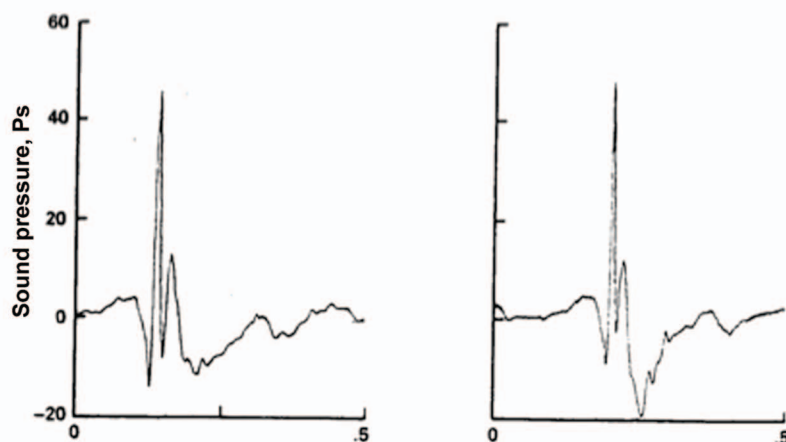
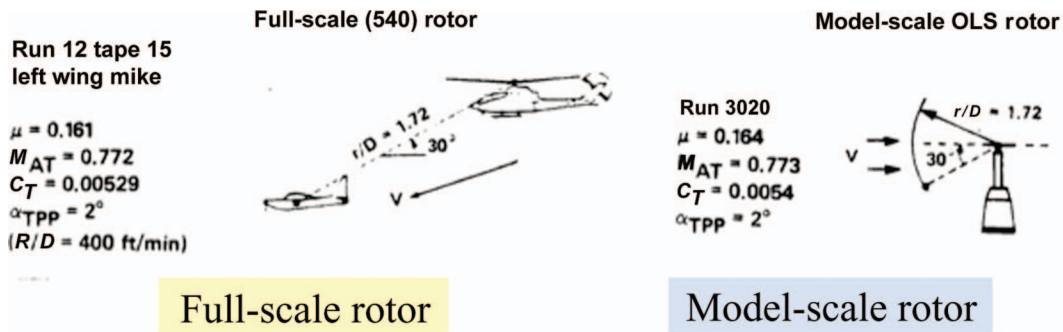


Fig. 42. BVI noise scaling at low to moderate advance ratios.

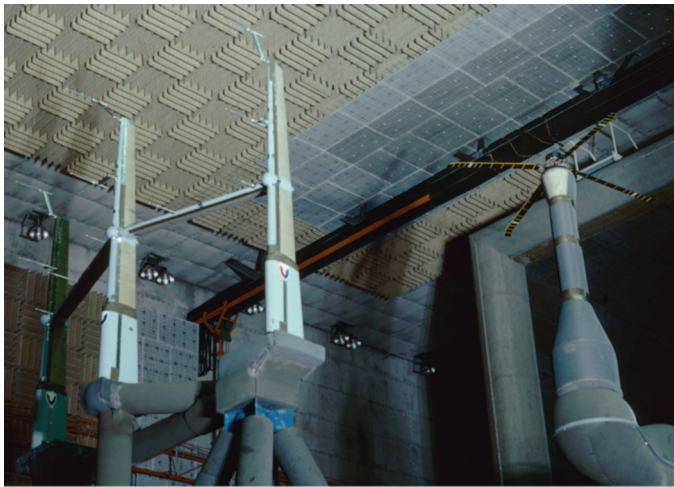


Fig. 43. UH-60 model-scale rotor in the DNW.

should utilize the full acoustic capabilities of the 40 × 80-ft wind tunnel to help further define the limitations of rotor scale-model testing.

First Principles Prediction

With good acoustic data in hand, in 2004, a large effort was undertaken to upgrade the country's CFD methodology with the goal of making accurate predictions of helicopter noise. Called the "Helicopter Quieting Program" and run by DARPA, CFD, structural, and acoustic codes were upgraded over a 3-year period by three competing industry/academic teams. The aerodynamic, structural, and acoustic predictions were compared with data taken on a model-scale four-bladed rotor, tested in the mid-1980s, in the DNW (Fig. 43) (Ref. 43). The expectation was that

the new CFD technology would accurately predict the radiated noise for this four-bladed rotor without empirical adjustments.

A typical theory/experiment comparison from the "Helicopter Quieting Program" is presented in Fig. 44 at a condition known to produce both thickness and BVI noise (Ref. 44). Nine time histories are shown. Of the three microphones in the plane of the rotor, one is in the direction of forward flight (microphone #1), one is 30° to the port side (microphone #4), and one is 30° to the starboard side (microphone #7). The remaining six microphones are located at the same azimuth positions, but in two planes passing through the rotor hub but angled downward 15° and 30° below the rotor.

The comparisons are quite revealing. In the plane of the rotor, thickness noise is well predicted (level and shape) at this moderate speed flight condition. The advancing tip Mach number for this case is 0.82, well below the delocalization Mach number. All of the prediction methods give good results in the plane of the rotor. Significant differences between the various codes are noted, but the general trends are still well captured. It should also be noted that some of the discrepancies could be due to the acoustic properties of the DNW wind tunnel at these microphone positions.

Low-frequency noise prediction under the rotor tip-path plane becomes worse as low-frequency loading becomes more dominant. The experiment, with a microphone located 30° below the tip-path-lane, shows a tendency to assume a more classical plus-minus pulse shape, whereas all of the theoretical plots do not completely capture this effect. It is not sure whether this is due to the acoustic properties of the wind tunnel or due to theoretical limitations.

At all of the microphone positions shown, BVI noise is not predicted very well. This observation is shown more clearly in Fig. 45 for the in-plane, straight ahead microphone position. At this time, it is still not known whether this lack of prediction accuracy is due to inadequate wake modeling, inadequate CFD methodology (including gridding techniques), inadequate structural modeling, or inadequate acoustic

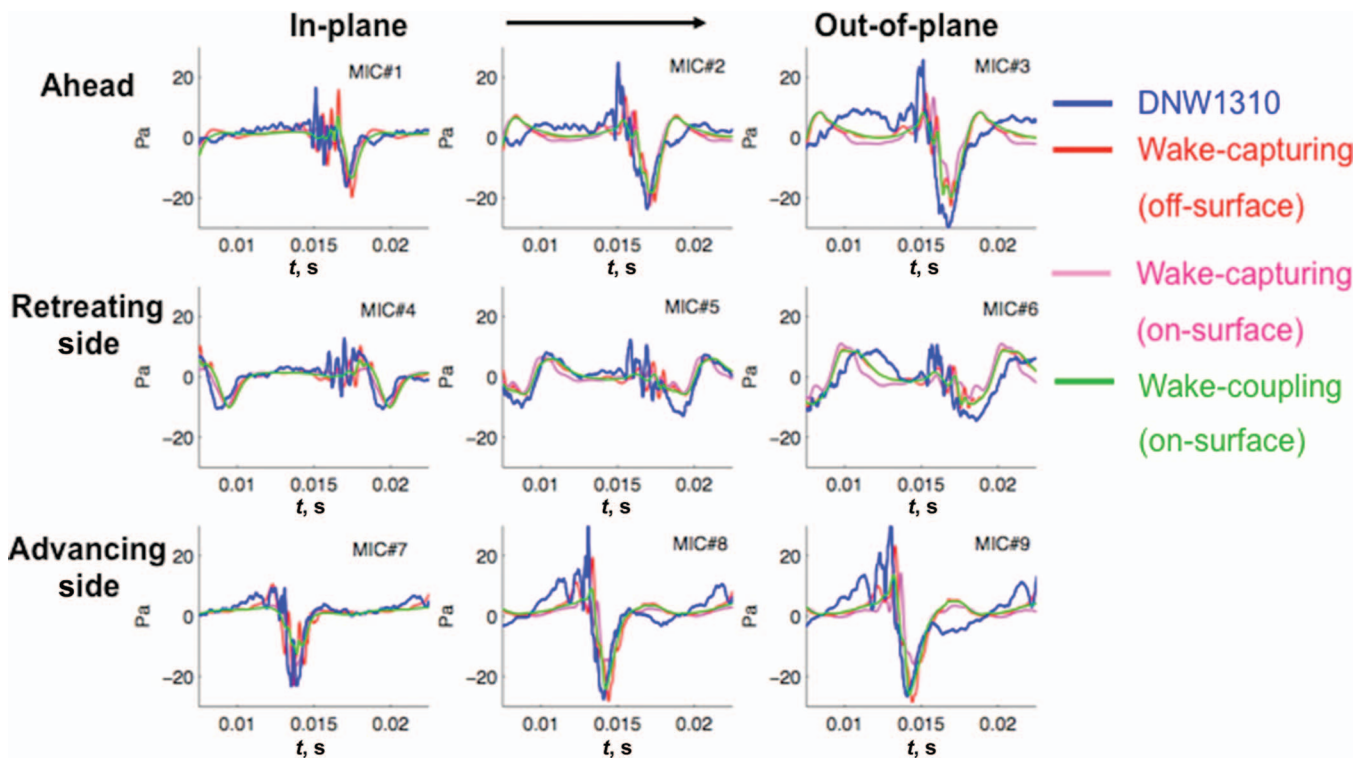


Fig. 44. Measured (DNW) and predicted (UMD) rotor harmonic noise for a four-bladed model rotor (one-fourth rotor revolution).

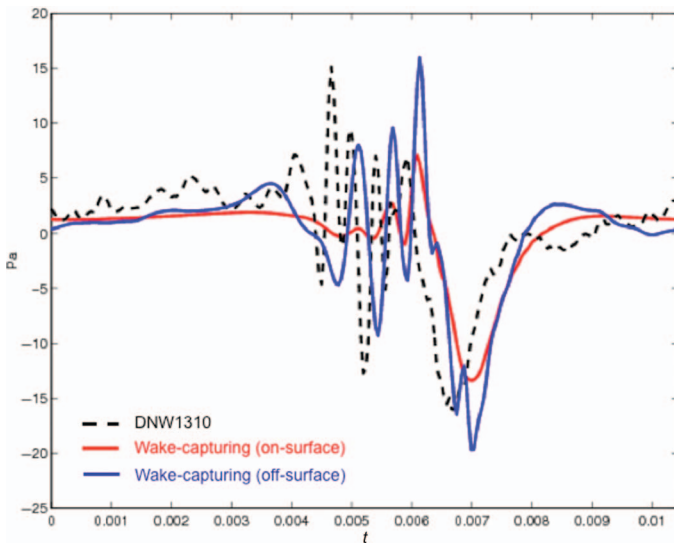


Fig. 45. Comparison of measured predicted BVI generated by a four-bladed model rotor in the DNW wind tunnel for a microphone located in the tip-path plane of the rotor in the direction of forward flight.

modeling. Current thinking is that the rotor wake's influence on blade loading is a primary factor in these less than good comparisons. It is clear that additional work is required to increase the ability of these codes to precisely predict BVI noise. This assessment may seem unfair—for no adjustment to the predictions to match the experimental data was allowed. But it was the overall goal of the “Helicopter Quieting Program” to not have to make such adjustments. It was hoped that computations would precisely match experimental data.

Matching theory and experiment is also made difficult by the size and complexity of the model-scale experiment. The rotors that were tested were designed to replicate the key parameters of a full-scale rotor. Geometry, tip-Mach number, advance ratio, and nondimensional thrust were chosen appropriately. The major structural properties of the blades were duplicated in the model-scale blades. However, the scaled model rotor could not duplicate the higher Reynolds number of the full-scale rotor. Model-scale blade fabrication inaccuracies also contributed to the poor comparison with theory, as verified by notable differences in blade-to-blade tracking and blade-to-blade BVI time histories.

It is still possible to gain a useful understanding of the BVI problem even if the details of the pulse shapes and levels do not compare that well with the measured acoustic data. Overall acoustic design, and operational trends can and have been explored in this controlled anechoic wind tunnel environment by many organizations over many years of testing. Parametric testing (wind tunnel and flight) has shown that keeping the rotor's wake as far from the rotor as possible will mitigate BVI. This will be addressed later in this paper.

The more general problem of CFD implementation for accurate BVI noise predictions is also being addressed—but it is a challenge. It is hoped that CFD will yield additional insight into the fundamental fluid mechanics of BVI, and that insight will lead to additional understanding and suggest new mitigation methods.

Blade-Controlled Disturbance Interaction

As discussed earlier, the key to reducing BVI noise is to weaken or diffuse the trailed tip vortex, weaken the rotor's response to the induced disturbances generated by the trailed tip vortices, or move the vortex

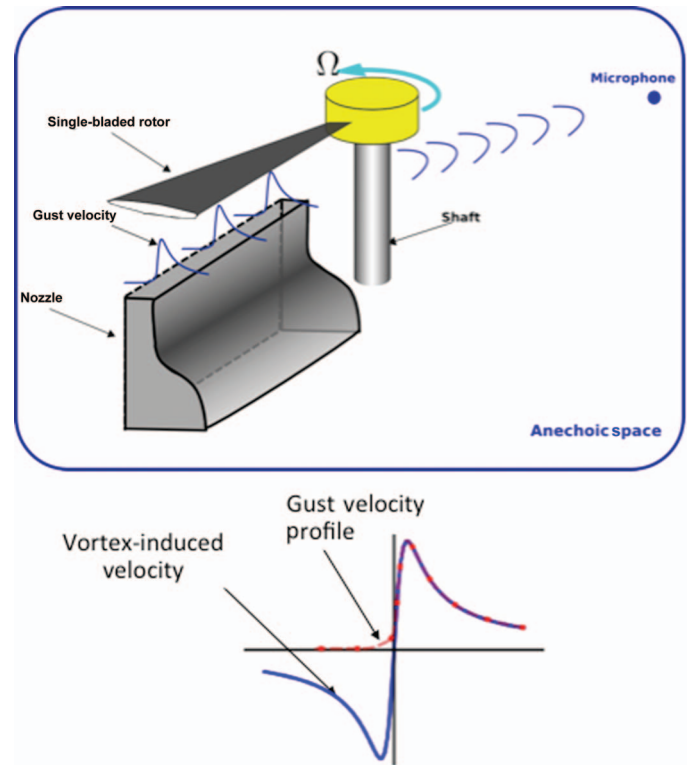


Fig. 46. Schematic of BCDI experiment (simulation of BVI).

trajectory away from the plane of the rotor. Over the years, serious attention has been given to try to weaken the strength of the tip vortices being shed through blade tip planform changes, subwings, active tip blowing, etc. It has been shown through full-scale flight-testing that about a 5–6 dBA (or PNL) noise reduction is possible (Ref. 17). Unfortunately, these BVI noise reductions normally adversely affect the performance of the helicopter, so their use to reduce BVI noise has been limited. Moving the trailed tip vortices away from the rotor tip-path plane can also reduce BVI noise—a topic that will be addressed later on in this lecture.

Another direct way of reducing BVI noise is to attempt to lessen the response of the rotor blades to sharp edge gusts. Rapid changes of pressure are lessened thereby reducing the BVI noise radiated by the helicopter. As has been discussed, quantitative correlation of BVI time histories with computations is complicated by scaling issues and by the fact that making a design change on the rotor may affect the strength and position of the shed tip vortices—thereby masking the desired cause and effect relationships.

The blade-controlled disturbance interaction (BCDI) simulation has been developed at the University of Maryland (UMD) to surmount these difficult experimental issues while focusing on the unsteady gust problem that is the core of BVI noise radiation (Refs. 45–48). As depicted in Fig. 46, the BCDI simulation consists of a one-bladed, untwisted hovering rotor operating at near zero thrust at full-scale tip Mach numbers. A two-dimensional like gust field is positioned near the rotor plane to provide a vortex profile that simulates the induced velocity field that would be produced by the helicopter's tip vortex. As the rotor blade passes through the stationary gust field, the major features of BVI noise can be simulated. The important governing parameters of this experiment are the rotor tip Mach number, the trace Mach number of the interaction, and the level and shape of the simulated two-dimensional vortex.

The stationary gust field is produced by carefully tailoring the flow through a specially developed nozzle. The nozzle has been designed to

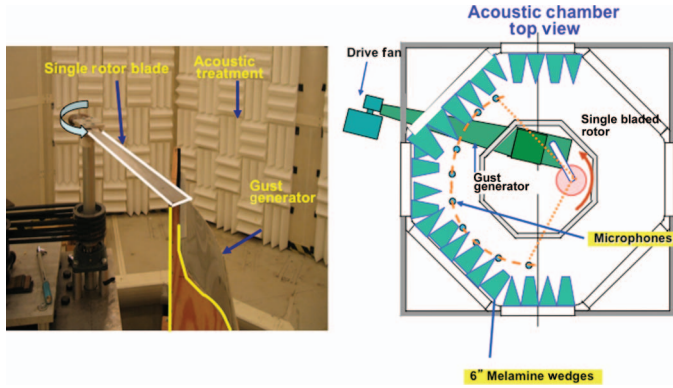


Fig. 47. BCDI experiment.

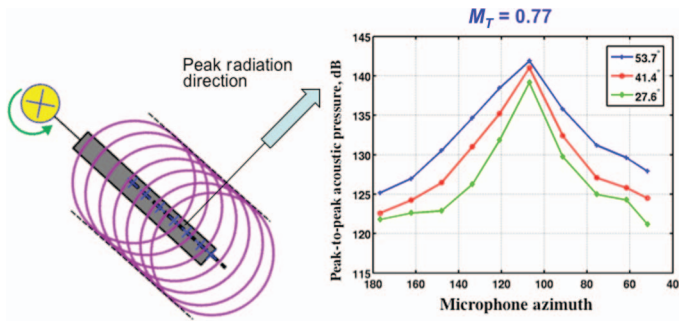


Fig. 48. Experimental measurement of peak-to-peak pressures for parallel BCDI ("broadside").

simulate part of the induced flow field that is produced by a line vortex, similar to one that is produced at the tip of a rotor blade. Because of experimental limitations, only the rising (front half) portion of the BVI profile can be simulated as shown at the bottom of Fig. 46. The nozzle can be rotated and translated in space to simulate BVI interaction angles and thus control the trace Mach number profiles of the interaction process. The nozzle can also be shaped to produce a curved line vortex to replicate the trace Mach numbers of the BVI. Because the strength and position of the velocity field can be controlled independently, the noise radiation caused by changes in blade design features, such as blade planform shape and airfoil design, can be assessed on a one-to-one basis.

The BCDI experiment is shown in Fig. 47 in the University of Maryland acoustic chamber. The single-bladed rotor and stand is mounted near the center of an acoustic chamber with additional wall wedges mounted on the walls in the path of the dominant first reflections. The gust generator nozzle is positioned close to the plane of the rotor as shown in Fig. 47. Because BVI is a high-frequency event, the acoustic chamber absorption qualities are adequate to minimize reflections from nearby surfaces. Microphones above and in the rotor plane measure the far-field BCDI noise. Background noise is low because the drive of the gust chamber is located outside of the treated acoustic space.

Typical BCDI measurements, shown in Fig. 48 for a parallel interaction profile (BVI # 3 for a typical two-bladed rotor), confirm the strong directionality of this type of BVI radiation (Ref. 48). The measurements also indicate that the radiation is strongest out of the plane of the rotor—indicating that the noise is dipole in nature. Figure 49 shows the detailed time history measurement of the interactions at the peak out-of-plane microphone position along with a comparison with two theoretical approaches that are typically used to predict BVI noise: indicial aerodynamic theory and a numerical simulation of the Euler equations using CFD. Indicial aerodynamic theory results, shown on the left-hand side of

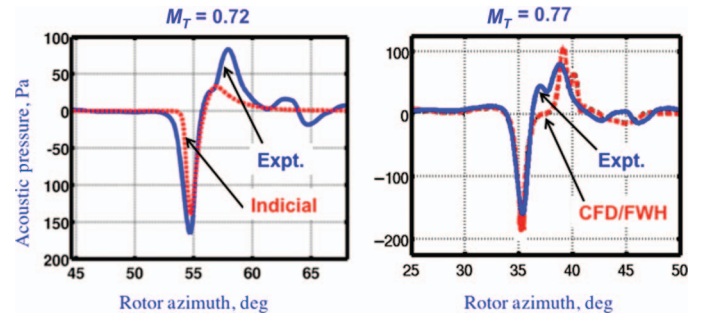


Fig. 49. Acoustic pulse shapes of parallel BCDI: Computation versus experiment.

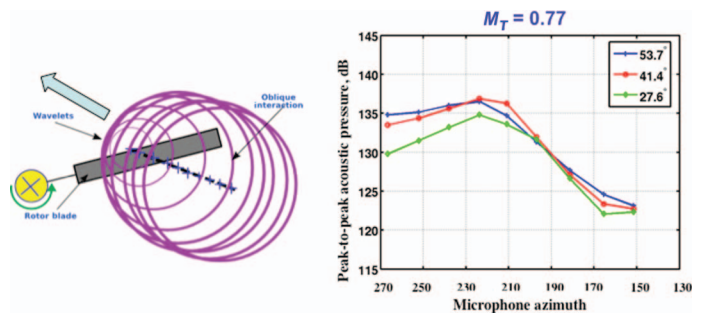


Fig. 50. Experimental measurement of peak-to-peak pressures for a typical oblique BCDI ("broadside").

Fig. 49, predict the negative portion of pulse shape for this parallel BCDI interaction, but cannot predict the positive portion of the pulse. The amplitude of the negative portion of the pulse is also under predicted for this compact chord acoustic model. CFD calculations show better agreement with the negative portion of the pulse (right-hand side of Fig. 49) and capture the general characteristics of the positive portion as well.

A sketch of the wavelet summation process for a typical oblique interaction (BVI # 2 for a typical two-bladed rotor) is shown in Fig. 50 along with the peak-to-peak acoustic pressures. For this case, the trace Mach number of the interaction begins supersonically and decelerates to subsonic Mach numbers. The strength of the simulated two-dimensional vortex field was held at the same value as the parallel interaction case. Although the peak amplitude of this oblique interaction is lower in magnitude by about 5 dB, the peak levels are spread over a much wider range of observer angles. The measured pulse shape of this type of interaction is shown in Fig. 51 along with the indicial and CFD calculations for two hovering tip Mach numbers. Once again, the indicial methods fail to capture the positive portion of the pulse shape, whereas the CFD is a better match to the measured data. Additionally, the CFD computation captures the general shape and level of the negative portion of the pulse, whereas the indicial method does not.

The BCDI simulation experiment provides some insight into these complex interactions. From this discussion, it is apparent that some method of representing unsteady rotor blade aerodynamics due to an unsteady disturbance field is essential to accurately predict rotor BVI noise. Apparent mass and shed vorticity effects resulting from changes in the induced velocity field need to be accurately represented. While the indicial approximations are helpful in capturing some of the effects of unsteady aerodynamics of BVI, they are most useful and accurate when the disturbance (vortex) and blade are nearly parallel to each other. For oblique interactions, the aerodynamic interactions need to be computed by methods that capture the three dimensionality of the BVI and the wake of the rotor. It is also apparent that phasing of the acoustic wavelets

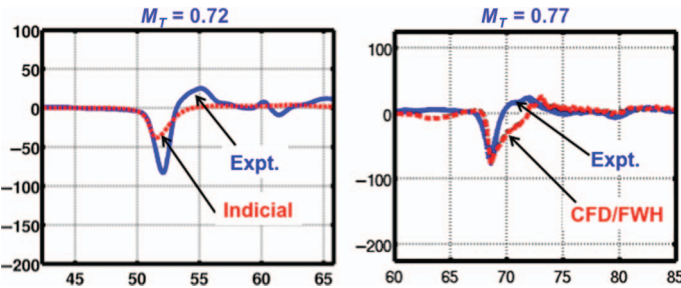


Fig. 51. Acoustic pulse shapes of oblique BCDI: Computation versus Experiment.

governs the strength, character, and directionality of BVI. Near transonic trace Mach numbers in the plane of the rotor, transonic aerodynamics may also influence the aerodynamics of the interaction and thus influence the radiating noise.

Methods of Rotorcraft Noise Control

Although a complete understanding of the factors that control the details of BVI noise are not completely known, enough information exists to devise designs and operational methods to avoid intense BVI. However, changes to design and operations to reduce BVI can come with some performance and increased vibration sacrifices. The goal is to obtain the most noise reduction while minimizing these detrimental effects.

Low tip Mach number rotors

Very early helicopters did not have very high tip Mach number rotors and did not radiate much high-speed helicopter thickness noise, although other noise sources, like unmuffled engines, often dominated their noise radiation. High tip Mach number rotor systems were developed during the Vietnam War era when the turbine engine, with its high power to weight ratio, began to power many helicopters. The major purpose of the helicopters developed during the Vietnam War era was to lift large payloads and carry them short distances to support and fight in unprepared areas. A large number of high tip Mach number rotor systems were developed that were optimized for these military missions. These same rotor systems were commercialized for use for commercial operations.

It is well known that reducing the high tip Mach number of helicopter rotors, either by design or operation, reduces helicopter thickness noise radiation substantially. In forward flight, this reduction can be achieved by flying more slowly or by reducing the operational RPM of the rotor and hence the tip Mach number of the rotor. However, reducing the hover tip Mach number requires blades with larger areas and consequently more weight to maintain the same thrust in hover. This, in turn, requires a rotor system with a higher torque and a higher weight helicopter transmission. For a turbine helicopter, hover and forward flight performance also depend upon the torque characteristics of the engine and the autorotation inertia criteria of the resulting rotor system. The net result is often a helicopter with somewhat poorer hover performance at similar gross weights.

Lowering the hover tip Mach number of a rotor system also reduces the helicopter's advancing tip Mach number—enabling the helicopter to fly faster in a more efficient manner until the advancing side of the rotor disk experiences adverse transonic aerodynamic events and/or the retreating side of rotor disk approaches stall. The increase of forward speed can improve the helicopter's forward flight performance and range. This was the case in the post-Vietnam era for the U.S. helicopter industry.

The design emphasis today is to try to optimize performance while avoiding excess helicopter external noise radiation.

It is interesting to relook at these noise/performance trade-offs in the light of the possibility of a helicopter electric drive propulsion system. The revolution in pure electric technology or in hybrid electric systems that is occurring in automobiles might someday occur in airplanes and helicopters. Because the torque of an electric motor is proportional to the current drawn by the motor, it is possible to develop high torque at low RPM without the use of heavy gearboxes. This may enable low RPM operation and hence lower helicopter noise levels.

As discussed previously, harmonic noise pretty much controls the noise levels of the modern helicopter. At high tip Mach numbers, thickness noise is dominant near the tip-path plane of the rotor. At lower tip Mach numbers, loading noise becomes dominant. This trade-off is shown in Fig. 52 for a hovering rotor of several thickness ratios, over a wide tip Mach number range, for an observer positioned in the tip-path plane of the rotor. The loading noise calculations are based upon steady lift and drag estimates of this hovering rotor. At lower tip Mach numbers, thickness harmonic noise decreases more quickly than loading harmonic noise levels. It is clear that the loading noise at lower tip Mach numbers is predominant and quite small.

This trend is generally valid for a rotor (or a propeller) with a constant loading distribution. However, if the loading varies as it does in helicopter forward flight, the reduction in loading harmonic noise will not be as much. The changes in lift and drag as the rotor rotates that are necessary to balance rolling moments on the helicopter in forward flight will also radiate harmonic noise. If these loading changes are small, not much additional harmonic noise will be generated. However, if the loading changes are abrupt, as in the case of BVI, significant harmonic noise will be generated.

As discussed previously, BVI noise is a function of how the acoustic disturbances arrive in time at an observer. The trace Mach number governs the strength and directionality of this noise. The tip Mach number of the rotor plays a more secondary role although lowering it still reduces radiated noise levels. The net result in general is that lower tip Mach number rotors produce lower levels of BVI noise, but not by as much as the steady loading arguments would suggest.

Lowering the tip Mach number of the rotor also uncovers other sources of rotor noise that have not been highlighted in this article. Broadband noise, due to wake proximity to the rotor, vortex shedding, atmospheric turbulence, or all of the above, adds to the radiated noise. While it is clear that more research into the noise/performance trade-offs at lower tip Mach numbers is needed, it is also clear that low tip Mach number operation can lower helicopter noise radiation substantially.

Blade planform, sweep, and leading edge serration changes to reduce BVI noise

Reducing the strength of BVI noise sources through blade planform changes near the tip of the rotor blades is somewhat effective in reducing BVI noise levels. An AH-1 helicopter outfitted with three different rotor blade sets was flown in formation with the YO-3A aircraft to measure BVI noise (Fig. 12) (Ref. 17). A nominal constant chord rotor was flown as baseline over a range of descent angles and advance ratios known to generate BVI. A specially designed 747 blade, that was thinned and tapered near the tip, was also flown along with a blade set with an “ogive”-shaped tip that radically reduced the planform area near the tip of the blade. Peak BVI noise levels and BVI dBA levels were reduced about 4–6 db from their maximum levels. It was postulated that the maximum strength of the tip vortices shed from the rotors with the modified planforms were responsible for these measured reductions. However, these BVI noise reductions were not free. Because the blade

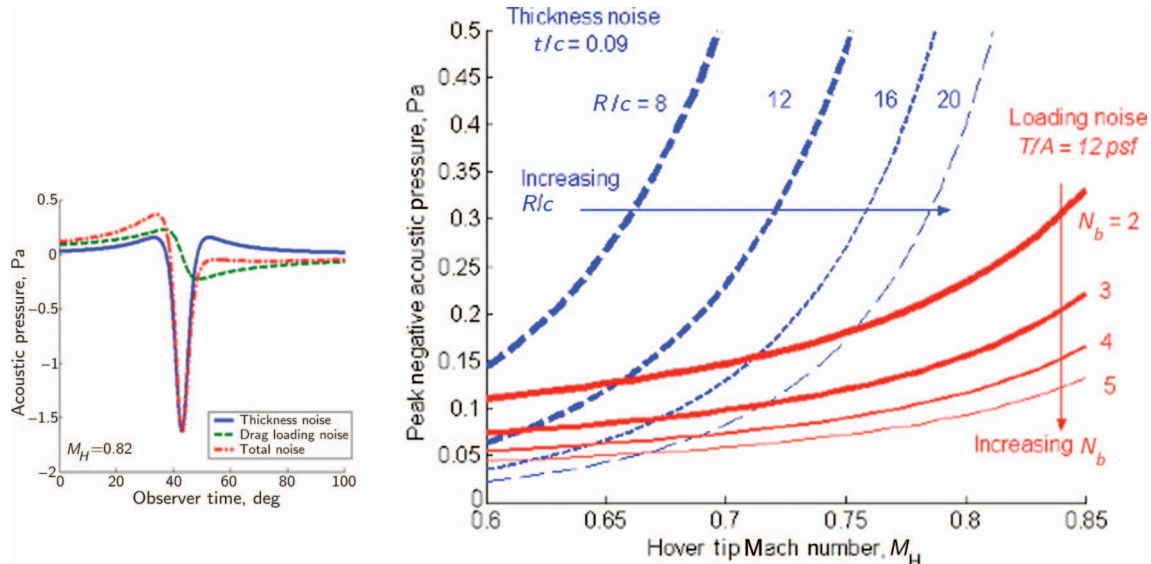


Fig. 52. Thickness and loading noise trade-offs for a hovering rotor of different aspect ratios: In-plane microphone.



Fig. 53. Eurocopter "Blue Edge" blade.

chord near the blade tip of the modified rotors was reduced, some hover performance degradation at high lifting conditions was also measured. These results confirmed what had been known from model testing—that reducing BVI while maintaining rotor performance over all flight-test conditions is difficult and that additional controlled experiments were needed to substantiate the acoustic/performance design trade-offs.

The shorter wavelength and deterministic nature of BVI pulse time histories can be used to some advantage by arranging the trigger points of the BVI acoustic events in such a manner that many of the plus/minus acoustic pressure disturbances cancel at a far-field observer—lessening the strength of BVI noise. Because BVI is mainly a leading edge event, altering the shape of the blade's leading edge can be effective at reducing BVI noise at chosen observer locations. This effect has been known for many years. A flight test of "Eurocopter's Blue Edge Blade" (Fig. 53) has confirmed that leading edge changes can be used to reduce BVI noise at chosen observer locations (Ref. 49). It is postulated that the forward backward sweep of the "Blue Edge Blade" encourages the BVI to be more oblique, which reduces the strength of the acoustic pulses while fostering cancellation at chosen observer locations.

Unfortunately, it is difficult to be more precise about what has been changed during the BVI that has changed the noise radiation. Changing the planform does change the phasing of the BVI but planform changes also change the blade aerodynamics, which could also influence the strength and shape of the radiating noise. In addition, changing the plan-

form is likely to change the shed tip vortex strength and resulting wake structure and thus further alter the BVI noise radiation.

As has been shown, the BCDI simulation can be used to uncouple the wake and the rotor blade response to disturbances to foster a better understanding of the factors that govern BVI noise radiation. A hovering rotor is made to pass through a stationary gust field that simulates parallel or oblique interactions, and acoustic data are recorded in an acoustically treated room at several microphone locations—both in and out of the rotor plane (Fig. 46). During the BCDI, no change to the disturbance field occurs due to changes in interaction disturbance strength or position. This ability to isolate the rotor response to a controlled gust field through the BCDI simulation offers a new way of understanding the effect of phase and unsteady rotor response to radiated BVI noise.

It has often been theorized that designing a rotor with a wavy or serrated leading edge could soften the response of the rotor to unsteady flow disturbances and hence reduce the radiated BVI noise. Two separate phenomena could act to cause this favorable effect: Each serration segment could act like a small delta wing and lower the effective unsteady response of that segment, and/or the chordwise time change in retarded time introduced by the serration could cause the resulting acoustic disturbances to arrive at the observer at slightly different times. When summed at the observer, the rotor's unsteady response to disturbances would be lessened when compared with a rotor with an unserrated leading edge response.

A theoretical attempt assessing the second effect is shown in Fig. 54 for a rotor intersecting an epicycloid line vortex. A peak-to-peak acoustic calculation, using indicial aerodynamics, of a straight blade and a blade with two sinusoidal leading edge chordwise variations is shown in Fig. 54. The basic theory shows that sinusoidal leading edge variations can alter the phase of each rotor blade segment and thus reduce the amplitude of BVI noise (Ref. 50). In these calculations, it has been assumed that each segment of the blade's unsteady response to flow disturbances is the same as the straight blade calculation.

Some additional favorable evidence of the effect of a wavy rotor was obtained experimentally by measuring noise of a "wavy blade"—a blade with large sinusoidal leading and trailing edge variations (Ref. 51). Acoustic power measurements were made in a wind tunnel with hard walls and with minimal acoustic treatment for wall reflections. Although overall noise power reductions were reported, it was impossible to discern quantitative features of the noise (directivity and pulse shapes) and to quantify the effect that waviness alone had on the radiation of BVI noise.

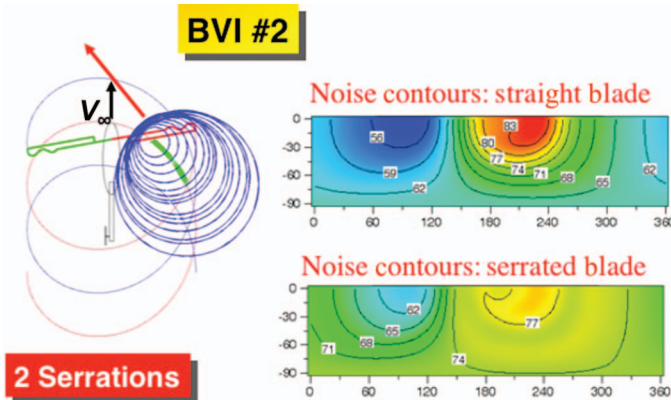


Fig. 54. Serrated blade phase cancellation effects on peak levels.

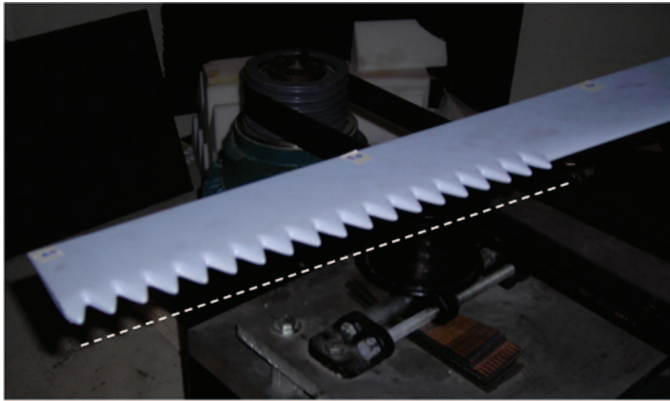


Fig. 55. Serrated leading edge blade (circa 1980).

A more recent test at the University of Maryland's Acoustic Hover Test Facility has confirmed that substantial BCDI noise reductions can be achieved by serrating the leading edge of the rotor blade (Ref. 52). Constructed in the early 1980s, the serrated rotor blade was not tested until a more quantifiable way of evaluating the acoustic effects of serrations was developed. The BCDI simulation of BVI, where cause and effect can be isolated, is one such method. A model-scale AH-1 rotor (Fig. 55) was built with a cross section whose leading edge varies sinusoidally, resembling a saw-tooth pattern, along the outer span of the rotor. The maximum deviation between the maximum chord radial station and the minimum chord variation was 20% of the average blade chord. The wavelength of the serrated leading edge has an amplitude of $\pm 10\%$ of the blade chord over the outer 40% of the blade span. The rotor was tested in the single blade configuration in the University of Maryland Acoustic Hover Chamber (Fig. 47) for both parallel and oblique interactions. As discussed previously, a single-sided gust was generated to represent one half of line vortex. The BCDI time history acoustic data were compared with data for a straight rotor blade with the same solidity. Simple indicial aerodynamics and CFD were also used as input to a linear acoustic code to predict the acoustics of the BCDI.

The experimental results are quite encouraging (Ref. 52). As shown in Fig. 56, the serrated blades reduce near parallel BCDI pulse amplitudes, in the direction of maximum BCDI, by up to 4 dB in peak amplitude—with lesser reductions shown in directions where the peak amplitudes are lower. Peak oblique interaction BCDI reductions (Fig. 57) for an oblique interaction angle are slightly smaller, 3 dB, but the reductions are spread to wider interaction angles than the parallel interaction case making the

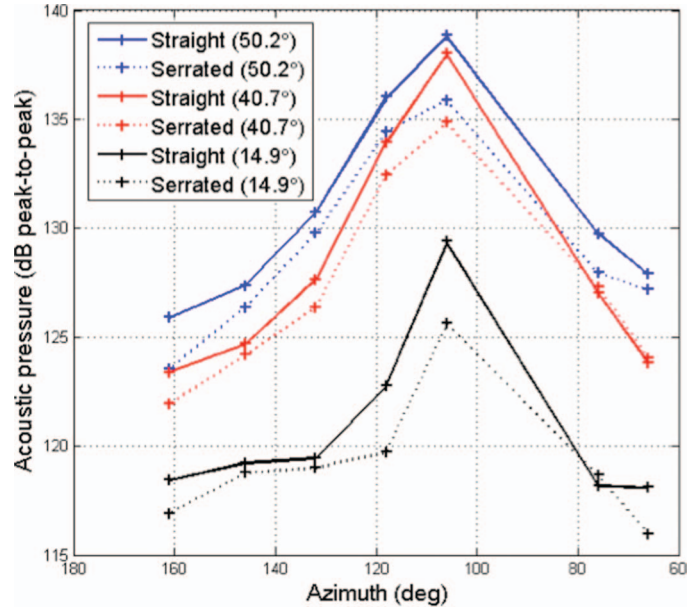


Fig. 56. Measured peak-to-peak sound pressure level comparison of a straight versus a serrated rotor blade undergoing a parallel BCDI.

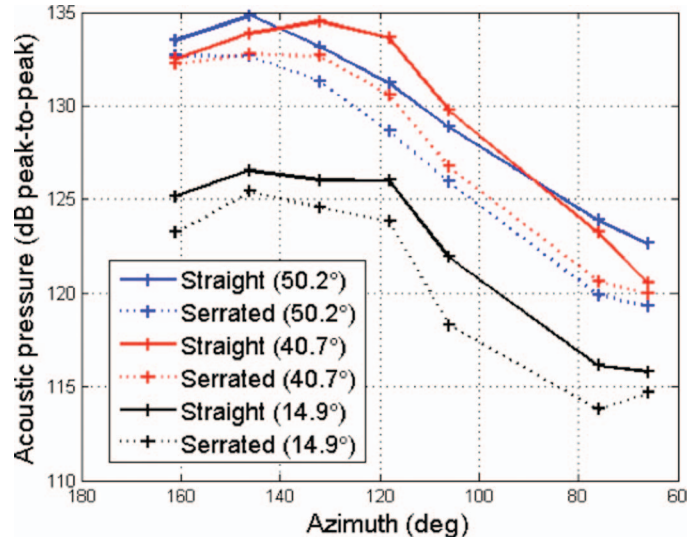


Fig. 57. Measured peak-to-peak sound pressure level comparison of a straight versus a serrated rotor blade undergoing an oblique BCDI.

reductions effective over larger directivity angles. As has been shown previously, BVI noise usually consists of many of these interactions—especially for rotor systems with many blades. Reducing each interaction by 3–4 dB would substantially reduce overall BVI noise.

It is clear that altering the leading edge of the blade to enhance phase cancellation of external noise can reduce BVI noise levels. However, the physical mechanism that causes this reduction in radiating noise due to the serrations is still not explicitly defined. Is it a reduction in the unsteady lift curve slope, and/or a changing phase of the disturbances that arrive at the observer? The net performance gain or loss in terms of lifting ability and performance loss/gain still needs to be quantified. Designing a serrated rotor blade that maximizes BVI noise reduction for both parallel and oblique interactions, which are likely to be seen during

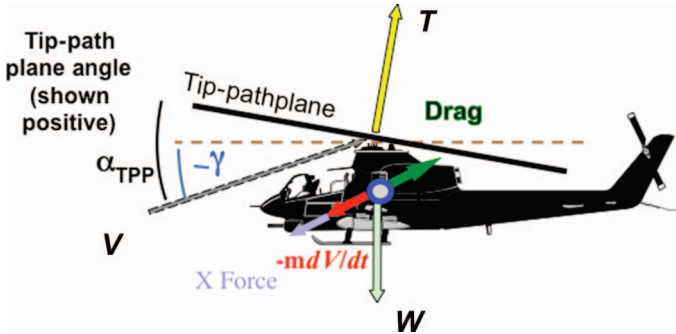


Fig. 58. Helicopter longitudinal force balance.

normal helicopter flight while minimizing rotor performance penalties, is a future challenge.

Blade-wake separation control to minimize BVI noise

Another way of minimizing BVI noise is to control the rotor such that the tip vortices, shed from the blades, do not pass in close proximity to the rotor. This effect was depicted in Fig. 37 for single main rotor helicopter. Keeping the rotor wake from coming close to the rotor's tip-path plane also minimizes the rotor's response to other self-generated aerodynamic disturbances and tends to reduce rotor noise in general.

Increasing the inflow through the rotor is a direct way of increasing the separation distance. This can be done by increasing the induced velocity of the rotor or by changing the inflow through the rotor by using tip-path-plane tilt. Increasing the induced velocity occurs when the thrust of the rotor is increased and is most effective at low forward speeds where the induced velocities are the highest. However, the increased thrust levels also lead to increased tip vortex strengths that can increase the noise. Changing the inflow by changing the orientation of the tip-path-plane angle with respect to the free-stream velocity vector is most effective at medium to high forward velocities where BVI is the most dominant source of noise.

In steady-state trim, wake geometry and a simple balance of forces in the *X* and *Z* directions, as depicted in Fig. 58, govern the longitudinal tip-path-plane angle of the main rotor. Summing forces along a wind axis system and assuming small angles, the governing equation simplifies to

$$\alpha_{TPP} = -\frac{D}{W} - \gamma - \frac{1}{g} \frac{dV}{dt} \quad (5)$$

where acceleration normal to the flight path has been neglected, *V* is the velocity of the helicopter along the flight path, *D* is the drag of the helicopter, γ is flight path angle (shown negative), dV/dt is the acceleration of the helicopter along the flight path, and *X* force is an extra force acting along the flight path that can be used to control the tip-path plane.

This simple quasi-static equation controls, for the most part, the vertical position of the shed tip vortices and hence the level of BVI noise radiation (Refs. 53, 54). In level steady-state flight, the drag-to-weight ratio determines the tip-path-plane angle of the helicopter. For most helicopters, this angle is small and negative, but increases negatively at high forward speeds. Acceleration parallel to the flight path also increases the tip-path-plane angle negatively, increasing the inflow through the rotor in a direction opposite to the thrust.

In steady-state flight at low-to-moderate forward speeds, the wake passes below the rotor's tip-path plane—but not by much. As the helicopter descends, the vertical descent velocity opposes the generalized downward velocity of the helicopter wake through the rotor's tip-path

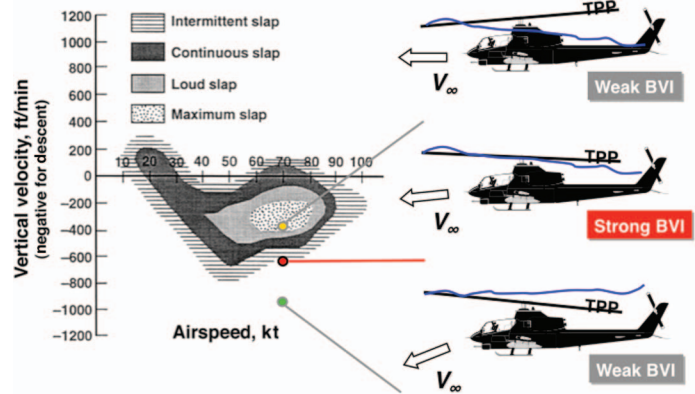


Fig. 59. The effect of steady descent rates on cabin BVI noise.



Fig. 60. In-flight, boom-mounted, Bell 206 in-flight noise measurement system.

plane, effectively moving the rotor wake closer to the rotor's tip-path plane. At some critical vertical descent rate, when the rotor blades are generally passing through the previously shed tip vortices, BVI is a maximum. Further increases in the descent rate cause the wake to pass above the tip-path plane and effectively reduce radiated BVI noise. This phenomenon is depicted in Fig. 59 along with a plot of what an observer would hear inside the cabin of a light-to-medium weight helicopter.

Data of this type were originally gathered by Bell helicopter in the 1960s (Ref. 55) and used to develop the Helicopter Association International's "Fly Quietly Program." A major message of that program to pilots was to fly the helicopter so as to avoid the most intense BVI noise as heard by pilots in the cabin. A "Fly Neighborly Guide" was produced for several models of helicopters (Ref. 56). Unfortunately, normal approach to landing procedures often placed the helicopter within this noisy region.

To quantify this effect further and to identify the directionality patterns of each type of BVI (oblique and parallel interactions), a series of special acoustic tests was performed with a Bell 206B helicopter (Ref. 57). The helicopter was instrumented with a specially developed tip-path-plane measurement system, an air data system, and a flying microphone measurement boom affixed to the skids of the helicopter as shown in Fig. 60. Acoustic measurements were made on the boom-mounted microphones and simultaneously on a ground microphone array. The pilot used specialized guidance to accurately control the flight path, and data were only taken with very low winds.

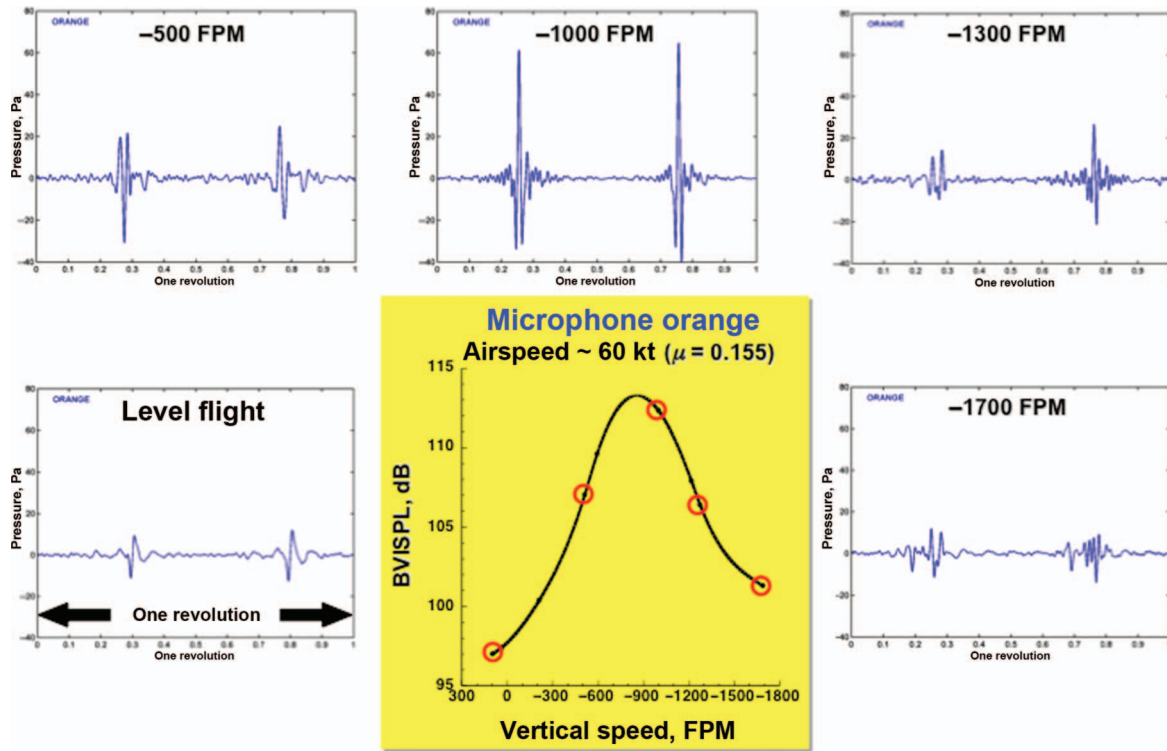


Fig. 61. Noise measurements taken on boom microphone to the advancing side of the Bell 206B helicopter.

Figure 61 presents the acoustic data taken on a boom microphone located on the advancing side of the helicopter in the direction of maximum BVI noise (Ref. 54). In general, the cabin noise measurement trends of Fig. 56 are confirmed. The BVI noise peaks to some maximum value as the descent rate is increased and then decreases as the rotor wake passes up through the tip-path plane. Time history and BVI sound pressure level (BVISPL) measurements are shown. BVISPL is the sum of the higher harmonic energy of the BVI pulse from the 6th to the 40th harmonic. BVI noise increases by as much as 15 BVISPL are noted in the direction of maximum BVI. Boom microphones in other directions generally show less dramatic but significant reductions.

The in-flight measurement testing also showed that the BVI noise heard in the cabin of the helicopter was not exactly the noise that was heard radiating away from the helicopter. As shown in Fig. 62, the most intense BVI region (yellow) is smaller and centered on a lower rate of sink than cabin noise measurements (gray) would indicate. A typical approach to a landing profile is superimposed on this figure in "red." A pilot first slows down and sets up an approach speed of 60–80 kt and a steady-state descent rate of about 500 ft/min ($\sim 6^\circ$ descent angle). He holds this condition until he flares and decelerates to the final landing point. As can be seen in Fig. 62, this normal approach has the helicopter generating strong BVI all the way down the constant descent angle flight path. The "Fly Neighborly" approach is also indicated in Fig. 62 in "blue." In this modified approach, the helicopter starts his approach at higher airspeed and significantly increases his rate of sink, forcing the wake up above the tip-path plane of the rotor, to reduce BVI noise radiation. The "blue curve" shows that the most intense BVI regions are avoided by using this procedure.

For practical operations, two additional factors need to be considered. The first is the observation that the BVI boundaries shown in Fig. 62 are, in fact, not as well defined as indicated. Piloting technique, bumpy air, winds, and wind gradients all influence the radiated noise and cause these boundaries to become fuzzy. The piloting implication is that the

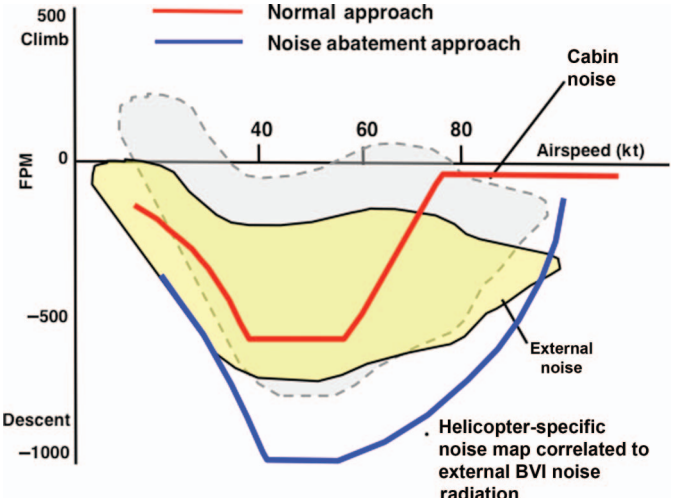


Fig. 62. Bell 206 Fly Neighborly Cabin Noise Guidelines and Measured External Noise Measurements.

pilot must maintain at least a 200–400 ft/min rate of sink margin to ensure that BVI noise is reduced. This requires even larger increases in the sink rate—often approaching the autorotation boundary of the helicopter. This leads to the second factor—that of maintaining adequate safety margins while flying the noise abatement procedures. Flying at these high descent rates to minimize noise while maintaining safety is not always possible. For this reason, these procedures have not gained favor with every helicopter pilot.

However, by altering the Fly Neighborly procedure somewhat, the margin required to decrease BVI noise can be increased and thus improve the overall safety of the landing approach procedure. As indicated in

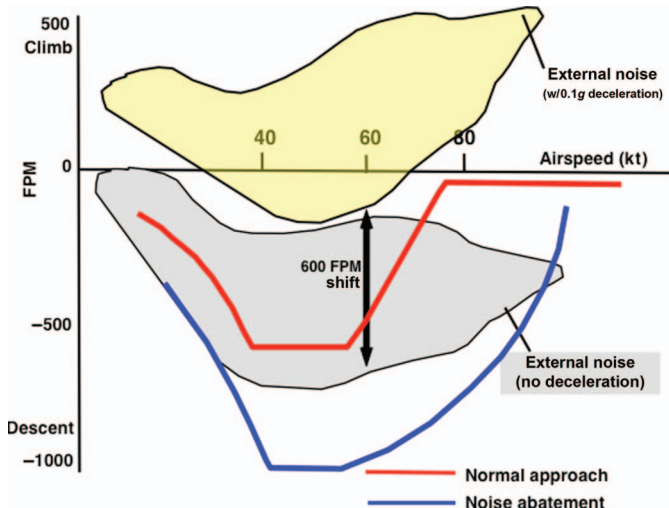


Fig. 63. Fly Neighborly guideline estimates with a 0.1 g decelerating approach.

Eq. (5), having the pilot accelerate or decelerate during his landing approach also can change the tip-path-plane angle and hence the inflow through the rotor (0.1 g deceleration is equivalent to a 5.7° change in tip-path-plane angle). Therefore, if the pilot decelerates at a constant 0.1 g parallel to his flight path during his descent, he substantially increases the inflow up through the rotor. This effectively moves the measured BVI region upward as shown in Fig. 63 resulting in larger buffer distances between the BVI region and the normal and noise abatement approaches. This larger distance between the BVI noise region and the flight path can be used to reduce the need to fly so steeply and therefore improve the safety of the noise abatement procedure.

Equation (5) also explains why BVI is not normally a problem during takeoffs. Accelerations cause the tip-path plane of the rotor to become more negative, increasing the inflow through the rotor in the direction opposite to the thrust. This pushes the wake far below the rotor to a flight condition where BVI is unlikely.

Sikorsky reported an example of the potential benefits that can be achieved by flight path management to mitigate BVI noise on their S-76 helicopter (Ref. 59). Measured ground noise profiles on an approach to a landing pad are shown for both a noise certification approach and a noise abatement approach in Fig. 64 for a microphone located along the centerline of the flight path. Flying a 9° descending 1.2 kt/s decelerating noise abatement approach reduces the peak BVI SPL noise levels by up to 11 dB. The extra margin afforded by using deceleration has lessened the requirement for very steep approaches to avoid BVI noise. Figure 65 presents the same results in terms of ground noise contour levels. The peak levels along the centerline of the flight path are substantially reduced with the benefits decreasing to either side of the flight path. It is clear that flight path management can achieve substantial reductions in noise on the S-76 helicopter on final approach to a landing but those reductions most affect the areas under the flight path and the immediate terminal area.

Correlating measured noise levels on the ground (Ref. 58) with pilot control and trajectory information are helping develop these improved noise abatement procedures. As discussed, cabin noise levels are not reliable indicators of noise radiation. A new opportunity currently exists to bring real-time noise radiation estimation into the cabin to help the pilot fly quietly. It is currently possible (or soon will be) to develop a predictive real-time acoustic radiation model of a particular helicopter that has as its basis measured acoustic data. This helicopter source model can then

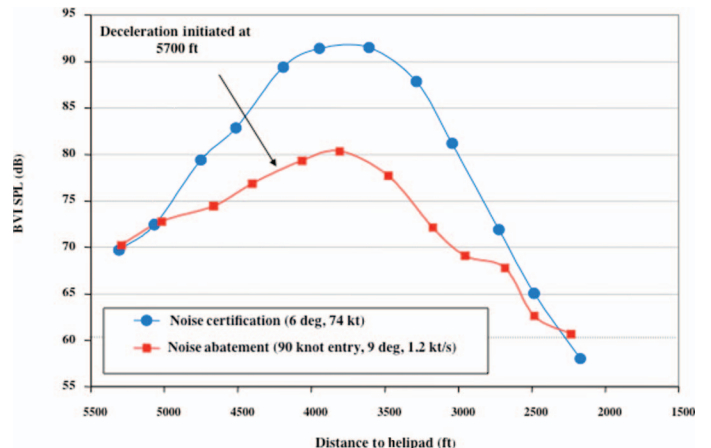


Fig. 64. Measured BVI SPL levels of a S-76 helicopter: Noise certification versus noise abatement approach.

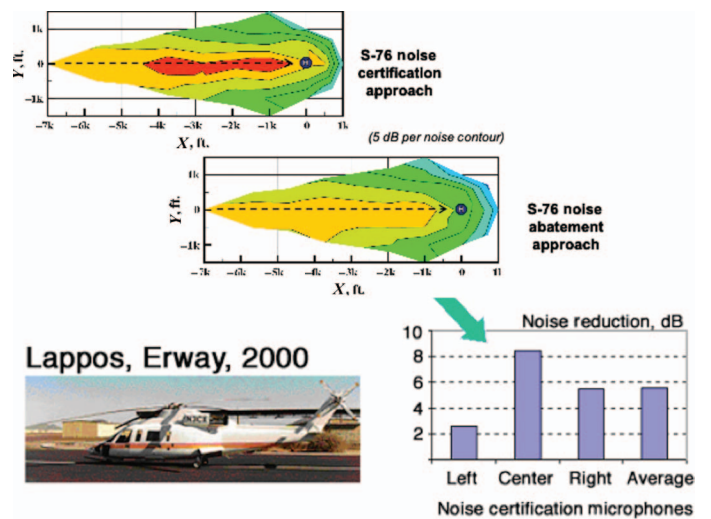


Fig. 65. Ground noise profiles of S-76 helicopter: Noise certification versus noise abatement approach.

be used for a variety of purposes including providing the pilot with real-time acoustic radiation contours that can be overlaid on a moving map ground display. These contours can be used to estimate detection distances contours and or helicopter annoyance contours to help the pilot improve his noise abatement flying skills. The noise modeling can also be used to help develop quiet flight path routing and control for both military and civilian applications.

There are several other methods of increasing the separation distance between the rotor tip-path plane and the rotor wake. Among the most effective is the use of an auxiliary force in the "X" direction—originating from a direct thrust or drag device (Ref. 53). This effect is shown schematically in Fig. 58. The resulting "X-Force" tilts the tip-path plane of the rotor, which can increase or decrease the inflow through the rotor thus affecting the distances between the rotor's tip-path plane and the shed wake. These types of propulsion devices are often found on compound helicopters and autogiros. The additional thrust in the drag force direction lets the rotor's tip-path plane tilt rearward causing the rotor's wake to pass above the tip-path plane of the rotor, thus mitigating BVI noise.

It should also be mentioned that there are on-blade active control methods that are being studied to reduce BVI noise. These methods try to

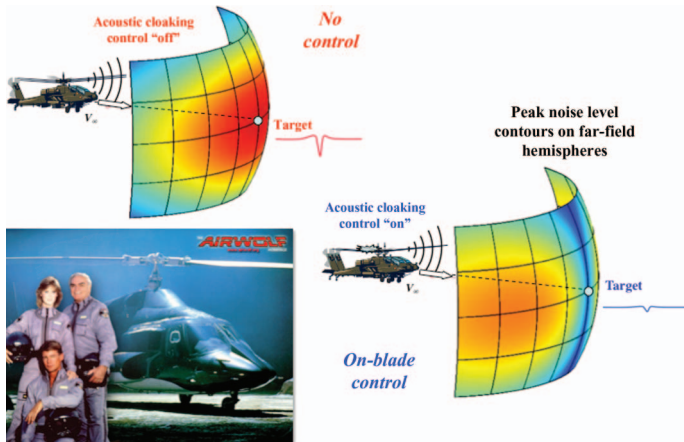


Fig. 66. On-blade active acoustic control concept.

decrease the strength of those tip vortices that interact with the following blades on the advancing side of the rotor disk where the most important BVI occurs. At the same time, the active control devices try to further increase the distance between the shed tip vortices and the following blades by warping the disk plane at important BVI disk locations. These methods rely, in part, on the warping of the tip-path plane so that each blade flies over or under specific shed tip vortices. Unfortunately, flying the rotor blades to obtain sufficient separation distance is difficult because the large centrifugal forces produced by the rotor keep the rotor blades close to the overall tip-path-plane angle. Relatively large out-of-plane thrust forces are required, and these can also reduce rotor blade performance and increase vibration. These forces also require the aircraft be retrrimmed which can move the tip-path plane of the helicopter—sometimes negating the acoustic benefit of the on-blade active control. Nevertheless, significant BVI noise reductions have been reported in controlled model-scale and full-scale acoustic wind tunnel tests. It remains to be seen if on-blade control can obtain similar noise reductions in flight and whether or not those gains are large enough to be operationally effective.

Active On-Blade Control of Thickness and Loading Noise

Thickness noise has a lower frequency content than BVI noise and is prevalent ahead of an approaching helicopter near the plane of its rotor. Thickness noise is important because it can often be heard above ambient noise levels and can give away the element of surprise. As we have seen, the shape of this pulse is governed by the thickness of the rotor blade near the blade tip and becomes dominant in forward flight at moderate-to-high tip Mach numbers. Because thickness noise is dependent only on the thickness distribution of the rotor, it is a very repeatable and steady periodic event at any given flight condition. These acoustic characteristics make it an excellent candidate for active phase cancellation. A key question to be asked was, *Can the thickness and force terms of the rotor noise governing acoustic equations be controlled in such a way as to reduce the thickness noise pulse, at a chosen observer location, ahead of an approaching helicopter?*

Work on this question began in 1998 by the author with some initial unreported results showing that the concept had merit. However, it was not until 2007 that quantitative computations showed that significant reductions of peak levels of thickness noise reductions were theoretically possible over a significant portion of the radiation field (Ref. 60). This analysis initially depended on a simpler explicit, but approximate, formulation of rotor noise that made theoretical optimization of the harmonic noise problem practical. A sketch of the on-blade active control concept

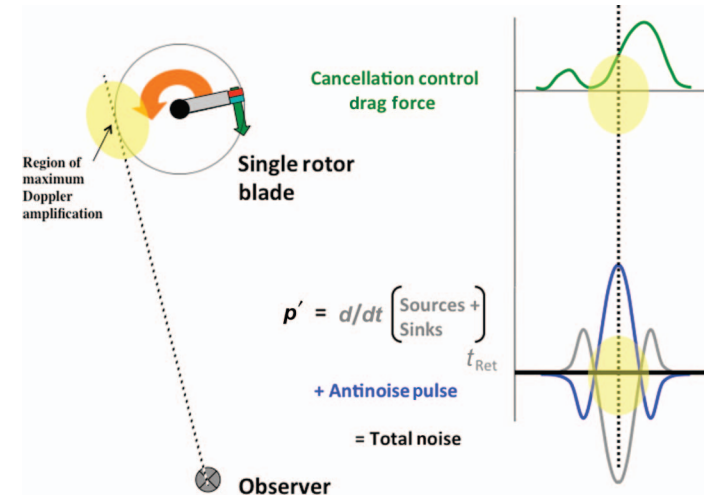


Fig. 67. Cancellation of thickness noise pulse shape through rotor drag control.

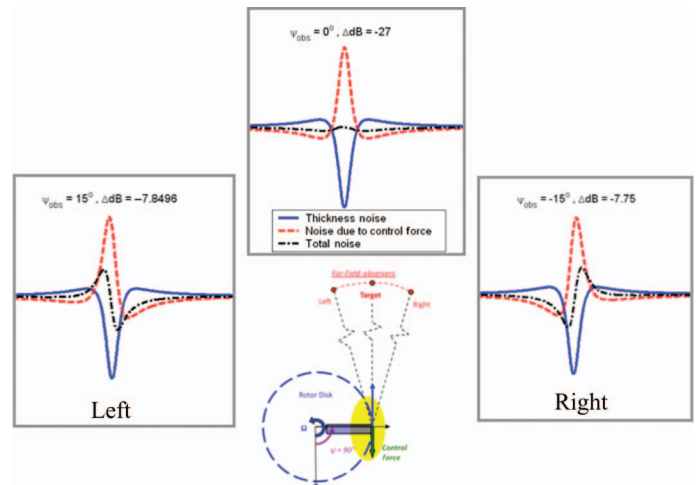


Fig. 68. Computed effectiveness of on-blade control of thickness noise.

is shown in Fig. 66 along with an insert from the once popular TV show, “Airwolf,” where such future technology to actively reduce rotor noise was taken as “poetic license.” The radiated noise field without active on-blade control is depicted in the upper left of Fig. 66. With the active acoustic control “on” (lower right of Fig. 66), the peak noise levels ahead of the helicopter are predicted to be significantly reduced.

The reduction concept makes use of active controllers on the rotor to produce time varying mass changes and time varying forces on the rotor to almost cancel the thickness noise radiation. The time derivative in the thickness and loading terms of the governing equations reduce the noise produced by rotor at a specific observer location. It should be noted that observers at other locations may see an increase in noise radiation levels. However, those locations are often not in important radiation directions and are therefore acceptable.

A key reason that on-blade control of thickness and loading is effective is that the cancellation relies on the same Doppler amplification factors that create the large thickness pulse. A sketch of the cancellation mechanism is given in Fig. 67 where an assumed time varying in-plane force (drag force) is controlled to produce an antinoise acoustic pulse that is equal and of opposite sign to the thickness noise pulse. In this case,

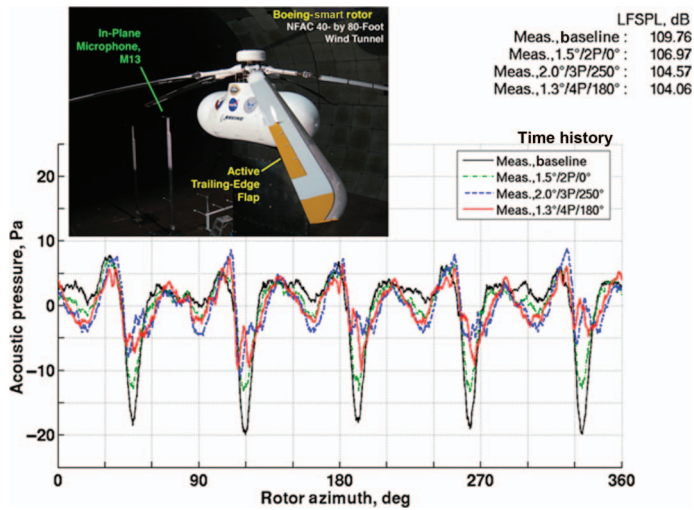


Fig. 69. Active flap control of in-plane thickness noise.

the in-plane force must increase when the rotor blade is at the azimuth angle corresponding to the maximum thickness noise position, on the advancing side of the rotor, near the 90° rotor azimuth location. The sum of the antinoise pulse and the thickness noise pulse is shown in Fig. 68 for three observer positions near the plane of the rotor. The thickness noise pulse is nearly nulled at the target position while to either side of this position the ability of the on-blade control to reduce noise diminishes. The narrowness of the pulse cancellation zone is typical for these types of active controllers and is a result of using the time derivative of the additional force and mass to cancel the rotor's harmonic signature (Refs. 61, 62).

There are several potential methods of creating the in-plane forces necessary for near in-plane low-frequency harmonic noise cancellation—including active flaps and active spoilers. A test that has yielded encouraging acoustic results and generally confirmed the concept of on-blade active noise control of harmonic noise, used active flaps to reduce in-plane thickness and loading noise (Ref. 63). This full-scale “Boeing SMART” (Smart Materials Actuated Rotor Technology) rotor is shown in the upper portion of Fig. 69 in the acoustically treated 40 × 80-ft wind tunnel. The closed test section wind tunnel is lined with a deep acoustic wedge system located behind a porous surface that effectively minimizes acoustic reflections from the tunnel walls for noise above about 100 Hz.

A typical result of this test is shown in the lower portion of Fig. 69 with several levels of active flap control. It is clear that using active flaps to control the forces near the tip of the rotor does alter the in-plane thickness noise time histories. The thickness noise peak levels are reduced by up to 50%. These data also reveal the difficulty of making low-frequency acoustic measurements on a large rotor in the 40 × 80-ft wind tunnel. Because of geometrical limitations of the wind tunnel, microphones are located close to the rotor (in the near acoustic field) and the low-frequency nature of large rotors cause some distortion of the overall thickness pulse shape—making quantitative measurements of the radiated noise difficult.

As discussed earlier in this paper, it is also possible to use a time varying mass control near the tip of the rotor to cancel thickness noise. This concept was explored at model scale using a specially designed non-lifting rotor blade in the University of Maryland acoustic hover facility shown in the left side of (Fig. 70) (Refs. 64, 65). The rotor was run at relatively high tip Mach numbers to generate thickness noise pulse shapes similar to those produced by a single-bladed nonlifting rotor in forward flight. As shown on the right side of this figure, without active on-blade

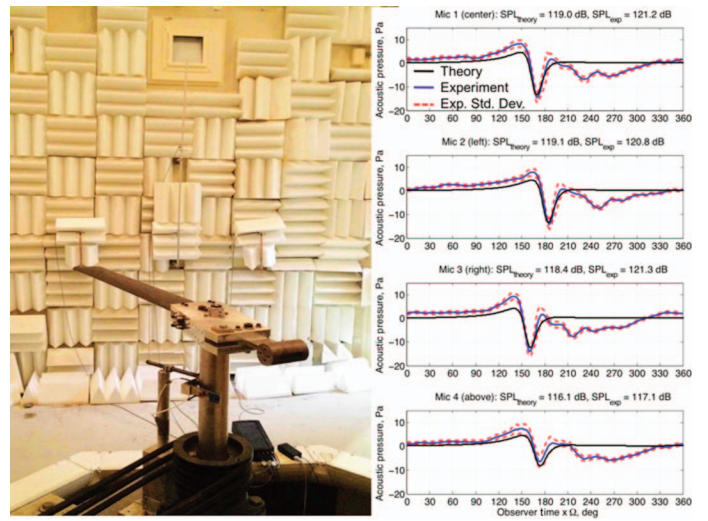


Fig. 70. Single-bladed rotor radial tip jet rotor in UMD acoustic chamber: Acoustic theory and experiment.

blowing control, theory and experiment match well in the University of Maryland facility.

The specially designed rotor blade was designed with internal ducting to pass air from the hub to the tip of the rotor. The air is supplied through a hollow rotor drive shaft and a pneumatic coupling in the rotor hub. A fixed frame high-frequency valve system controls the net mass flow that passes through the rotor hub to the rotor tip where it exits with subsonic velocities in the radial direction. As discussed earlier, the net mass flow exiting the tip is controlled to produce antinoise to reduce the thickness noise of this hovering rotor.

Similar to active flap control of drag, an increase in the mass flow rate exiting the tip of the rotor produces the pulse shape that reduces thickness noise. The antinoise generation pulse is generated by controlling the time history of the air that exits the tip of the rotor. The antinoise pulse acts through both the mass and force terms of the governing acoustic equations. Measured and predicted results with the active control implemented are shown in Fig. 71. Good agreement between theory and experiment, at four near in-plane microphone measurement positions, is shown—demonstrating that the governing theory is viable.

Although good reductions in thickness noise levels in the primary observer location are shown, reductions to either side of the pulse are not as good, as predicted by theory, and confirm that there is a defined region of effectiveness for active acoustic controllers (Ref. 65). These plots also show that the width of the active control pulse is not wide enough to cancel the measured pulse in this model rotor experiment. A key limitation of this experiment is the ability to pass enough mass flow through the control system to produce a large and wide enough active noise cancellation pulse shape. Small rotor ducting and adequate high-frequency control limitations have limited these results. To get around these model-scale limitations, the concept of using tip mass blowing to reduce rotor in-plane rotor noise is being pursued at larger scale.

It is clear that active on-blade control of in-plane harmonic noise is possible. What remains to be shown and demonstrated is that this concept can be a practical solution to the in-plane harmonic noise radiation problem.

Concluding Remarks

This paper has emphasized the basic nature of the noise generation process and has emphasized recent research and developments that led to an improved physical understanding and possible control of the dominant

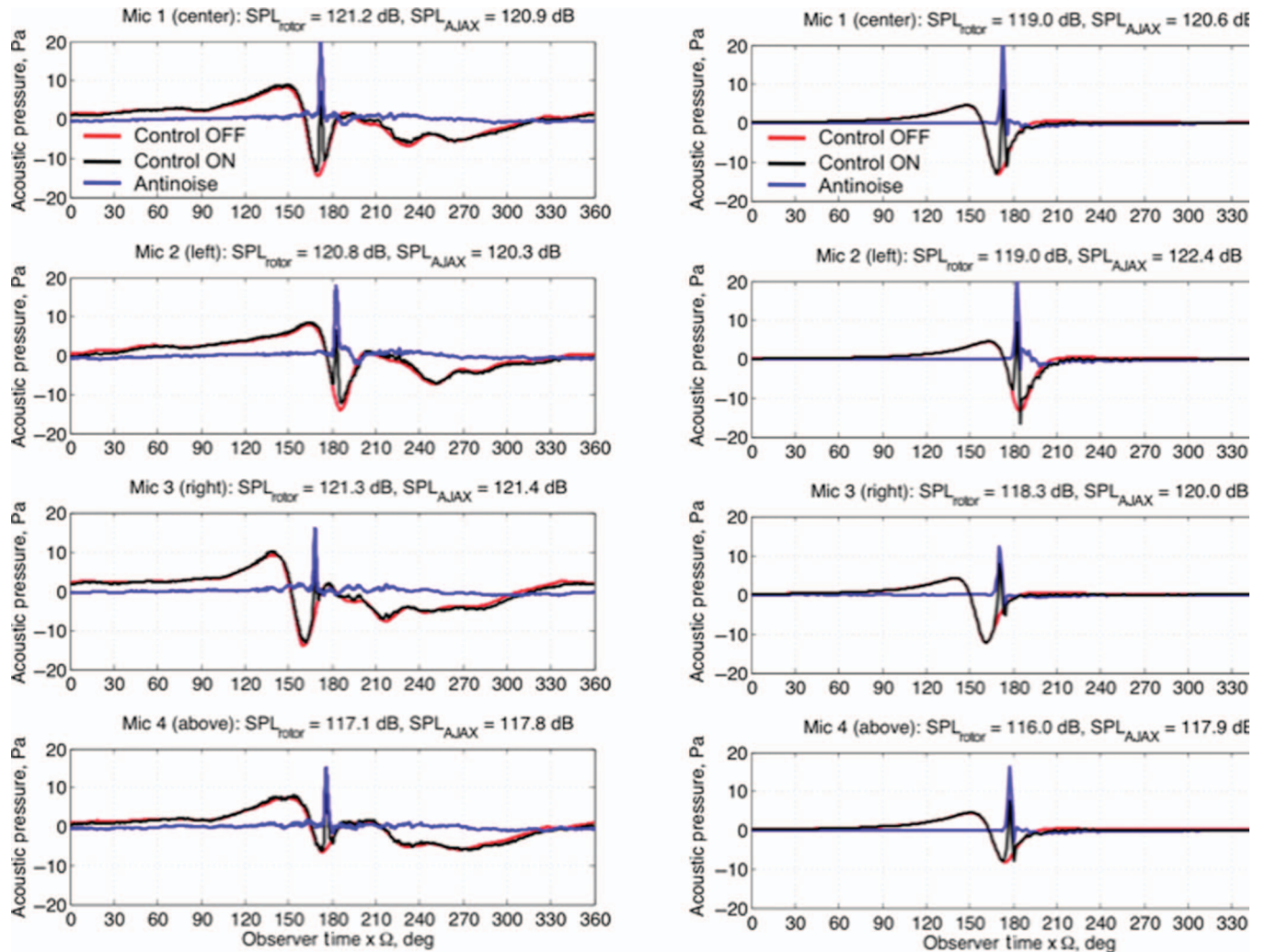


Fig. 71. Measured noise: Active on-blade tip blowing control.

sources of helicopter noise. In conclusion, it is also important to address the practical aspects of this work by asking the following questions.

How will understanding rotor noise generation mechanisms and control of these mechanisms lead to quieter helicopters?

To some extent, the knowledge gained from many years of rotorcraft noise research and operational experience has already been incorporated in today's modern helicopter. The fact that today's helicopters generate harmonic noise by rotating blades at high tip Mach numbers is responsible for much of the noise radiation. The noise is generated both by blade thickness and by steady and unsteady blade lift and drag forces that create unsteady disturbances in the air. When these flow disturbances are added and propagated to a far-field observer, the high tip Mach number of the rotating blades amplifies them to create high levels of harmonic noise. Consequently, the reduction of the helicopter's operational tip speed (tip Mach number) has been and still is the primary method employed by helicopter manufacturers to substantially reduce harmonic noise radiation.

Reducing the tip speed (tip Mach number) of the modern helicopter often requires other important design and mission trade-offs. If hover performance is the primary design objective, then having a high tip speed to maximize payload at a given gross weight is a logical consequence. The Vietnam era helicopters, with their high operational tip speeds, capitalized on the extra performance gained from these high tip speeds to

move heavy payloads short distances over unprepared terrain. However, lowering tip speed to reduce noise radiation is often bounded by design and safety considerations. Too much reduction requires high solidity rotors that may not be efficient in cruise and require additional mass weights at the rotor tips for autorotation.

The modern helicopter design has hover performance and cruise performance more equally weighted. This encourages lower hover tip speeds (with higher solidity rotors to maintain lift) to avoid excessive advancing tip Mach numbers. The result is a net reduction of rotorcraft noise over the operational envelope of the helicopter. Increasing the number of blades and consequently reducing the net thickness and tip vortex strength shed from each blade tip has also helped reduce noise radiation levels and, more importantly, has reduced the distinctive low-frequency "pop-pop" helicopter sound. However, increasing the number of blades has effectively increased the fundamental frequency of the noise radiation and can sometimes make the resulting sound more sensitive to human annoyance.

Helicopters that can operate at several operational speeds are also now appearing in the industry. Low tip speeds are used in situations where noise radiation is to be minimized, whereas higher lifting performance can often be achieved by operating the helicopter at higher tip speeds. Multispeed transmissions and modern control and design technology are facilitating the use of variable-speed rotors—to ensure safe operations at these lower tip Mach numbers.

What are the near-term technical challenges that can be applied to further reduce source noise?

Reducing the detection distance and community annoyance are the current foci of further noise research. Low observability, or minimum detection distance, requires that the lower frequency harmonic, near horizon helicopter noise, be reduced—the type of sound that can be distinctly heard above background noise levels. Flying slowly and reducing advancing tip Mach number reduce thickness noise and in-plane force (drag) noise—key contributors to near horizon harmonic noise. Reducing the hover tip Mach number of the rotor also reduces the advancing tip Mach number at the same forward speed and also reduces harmonic noise. However, flying at reduced RPM can push safety margins for autorotation. Providing the automation and control guidance to permit flight at low operational RPM is a near-term technical challenge that can lower noise levels.

Helicopter annoyance levels are governed by higher frequency noise sources. The dominant main rotor noise source near population centers for light-to-medium helicopters is BVI, which contains high levels of high-frequency harmonic noise. Increasing the separation distance between the shed wake of the rotor and the blades (tip-path plane) by flight trajectory management, reducing the strength of the tip vortices by tip design, the use of a larger number of rotor blades, and reducing tip speeds have been shown to reduce BVI. However, to be effective under nonideal situations, these separation distances have to be substantial. Providing automation and/or guidance to help the pilot to safely perform these noise reduction maneuvers is a near-term technical challenge.

Tail rotor noise is also important for detection and annoyance. Because the tail rotors spin at much higher frequencies than the main rotor, the important harmonic frequencies are shifted higher—making the lower harmonic noise of the tail rotor higher in frequency than the harmonic noise of the main rotor. Even though the absolute levels are reduced for this smaller rotor at the same observer location, tail rotor harmonic noise can be important for both annoyance and detection. As in the case of main rotors, adding more tail rotor blades with thinner tips and high-lift airfoils helps in reducing tail rotor harmonic noise. Designing tail rotors that can meet the performance requirements of the helicopter at lower tip speeds is another near-term technical challenge.

Computational advances (both in software and hardware) have been dramatically increasing the development of CFD as applied to rotorcraft. Developing and adapting these codes to predict far-field acoustics of rotorcraft has been and is an on-going technical challenge. Validating these codes so that they can be used to accurately predict helicopter noise radiation is another near-term technical challenge.

What are some promising new technologies that might be used to further reduce helicopter noise?

It has been shown that low-frequency harmonic noise levels can be reduced through active on-blade noise cancellation technology. This promising new research area uses the physics of the harmonic noise generation process to radiate “antinoise” in specific directions to lower radiated harmonic noise levels. More basic and applied research is required to further substantiate the benefits and compromises of this revolutionary technology.

Further reducing the operational hover tip Mach number of the helicopter is another good way of reducing harmonic noise radiation. (As mentioned, some of the noise reduction noted on today’s helicopter has been achieved through rotor RPM reductions.) Lower hover tip speeds at the same forward speeds require high advance ratio flight and are limited by stall on the retreating side of the rotor disk. These benefits require new research and designs that must overcome retreating blade stall either

through active blade technology or through adding additional winged lift on the vehicle.

Changing blade planform and/or leading edge geometry can be used to reduce peak levels of BVI noise radiation. While the basic physics of the mechanisms involved are still being explored, a potential for significant noise reductions seems realizable. New experimental approaches that isolate the governing physics in a controlled laboratory environment are necessary to isolate “cause and effect.” The performance gains/losses also need to be assessed over the helicopter’s flight envelope.

Knowing how much noise that is actually being radiated by the helicopter to the far field is important operationally for detection and annoyance reduction. At the present time, pilots do not have real-time knowledge of the directionality and level of rotor noise that is being radiated by the helicopter. The pilot is left to make this judgment by listening to noise in the helicopter cabin—an unreliable indicator at best. Pilots then use this unreliable audio information to judge detection distances and ground annoyance levels and to improve their fly quiet piloting skills. It is time to move to a new paradigm—one that utilizes reliable estimates of radiated helicopter noise levels as a function of flight condition and presents this information to the pilot in real time. A simple moving map display, similar to GPS systems now used in automobiles, that overlays predicted ground noise contours on the surrounding topography, will help the pilot maneuver to avoid radiating noise in particular directions. Such a system would also help the pilot improve his noise abatement piloting skills by providing direct cause and effect acoustic feedback. This same information could be used to develop a future flight planning routes that minimize aural detection and annoyance to the surrounding communities.

It has been shown that maximizing the miss-distance between the rotor wake and the rotor blades is a good way to minimize BVI and wake interaction noise. Introducing forces along the X-axis in a wind axis system to position the rotor’s tip-path plane helps control the miss-distance. Longitudinal acceleration/deceleration, thrusters/decelerators along the X axis, and flight path management are effective noise reduction methods that apply this principle. The next generation of rotorcraft will likely have some thrust devices that act along the X axis to help achieve higher forward flight speeds. These devices can be used to fly quietly by trimming the helicopter so that the rotor tip-path plane is positioned to be at larger distances from the shed tip vortices and thus avoiding the known conditions for BVI.

CFD technology is becoming an important tool in the rotorcraft design and development process. It is being refined and validated to help understand the complex flow environment of rotorcraft. Expanding this technology in such a way that it enters into the creative conceptual design process at the fundamental level is a higher level challenge. This new approach will help ask the question: What are the new designs and/or concepts that can reduce rotorcraft noise?

Author’s update

It has been nearly 7 years between when this paper was presented and its publication—something that I sincerely apologize for. Fortunately, acoustic research and development have continued with many results being incorporated in the helicopters of today.

The advent of the electric helicopter has put a new emphasis on low RPM and hence low tip Mach number rotors. High torque electric drive motors foster lower low tip Mach number rotor designs that substantially reduces the helicopter harmonic noise radiation due to thickness and places more emphasis on noise due to steady and unsteady loading. It also requires more rotor solidity (blade area/disk area), which will generate more broadband noise levels. These lower hover tip Mach number designs are challenged by the retreating blade aerodynamic stall

problems of high-speed flight. A new look at the noise radiation from these configurations is currently underway.

Controlling BVI noise has proceeded on many fronts. New blade tip shapes, control of the separation distance between the rotor tip-path-plane and the rotor wake, and computer control of flight trajectories have been demonstrated in many flight programs. The important remaining issue is whether or not these methods offer robust solutions to the BVI noise problem under nonideal flight conditions.

Active control of in-plane thickness noise through tip blowing has been successively demonstrated at model scale. New efforts to implement this technique are underway for military applications.

Acknowledgements

Many people have made this presentation possible. Dr. Gaurav Gopalan, my first Ph.D. student at the University of Maryland and my dear friend, was both an inspiration and major contributor. His unfortunate, untimely death was difficult for me and is definitely a loss to the entire rotorcraft acoustic community. Dr. Ben Sim and Dr. Sud Koushik, my colleagues and friends, were major contributors. Rick Sickenberger, Eric Greenwood, and Cal Sargent, recent Ph.D. graduates also provided technical contributions and assistance with the lecture and with the final manuscript.

References

- ¹Stepniewski, W. Z., and Schmitz, F. H., "Possibilities and Problems of Achieving Community Noise Acceptance of VTOL," *Aeronautical Journal*, Vol. 77, (750), June 1973, pp. 311–326.
- ²Cox, C. R., "Subcommittee Chairman's Report to Membership on Aerodynamic Sources of Rotor Noise," Preprint No. 625, American Helicopter Society 28th Annual Forum Proceedings, Washington, DC, May 17–19, 1972.
- ³Lowson, M. V., and Ollerhead, J. B., "A Theoretical Study of Helicopter Rotor Noise," *Journal of Sound & Vibration*, Vol. 9, (2), March 1969, pp. 197–222.
- ⁴Wright, S. E., "Discrete Radiation from Rotating Periodic Sources," *Journal of Sound and Vibration*, Vol. 17, (4), August 1971, pp. 437–498.
- ⁵George, A. R., "Helicopter Noise: State-of-the-Art," *Journal of Aircraft*, Vol. 15, (11), 1978, pp. 707–715.
- ⁶White, R. P., Jr., "The Status of Rotor Noise Technology," *Journal of the American Helicopter Society*, Vol. 25, (1), January 1980, pp. 22–29.
- ⁷Henderson, H. R., Pegg, R. J., and Hilton, D. A., "Results of the Noise Measurement Program on a Standard and Modified OH-6A Helicopter," NASA TN D-7216, September 1973.
- ⁸Robinson, F., "Component Noise Variables of a Light Observation Helicopter," NASA CR-114761, 1973.
- ⁹Schmitz, F. H., and Boxwell, D. A., "In-Flight Far-Field Measurement of Helicopter Impulsive Noise," *Journal of the American Helicopter Society*, Vol. 21, (4), October 1976, pp. 2–16.
- ¹⁰Schmitz, F. H., Boxwell, D. A., and Vause, C. R., "High-Speed Helicopter Impulsive Noise," *Journal of the American Helicopter Society*, Vol. 22, (4), October 1977, pp. 28–36.
- ¹¹Schmitz, F. H., Boxwell, D. A., Dahan, C., and Lewy, S., "A Note on the General Scaling of Helicopter Blade–Vortex Interaction Noise," ONERA T.P. No. 1982-32, May 1982.
- ¹²Boxwell, D. A., and Schmitz, F. H., "Full-Scale Measurements of Blade–Vortex Interaction Noise," *Journal of the American Helicopter Society*, Vol. 27, (4), October 1982, pp. 11–27.
- ¹³Boxwell, D. A., Schmitz, F. H., Spletstoesser, W. R., and Schultz, K. J., "Helicopter Model Rotor–Blade Vortex Interaction Impulsive Noise: Scalability and Parametric Variations," *Journal of the American Helicopter Society*, Vol. 32, (1), January 1987, pp. 3–12.
- ¹⁴Martin, R. M., Spletstoesser, W. R., Elliott, J. W., and Schultz, K. J., "Advancing-Side Directivity and Retreating-Side Interactions of Model Rotor Blade–Vortex Interaction Noise," NASA TP-2784, AVS-COM TR 87-B-3, 1988.
- ¹⁵Martin, R. M., and Hardin, J. C., "The Spectral Characteristics of Rotor Blade–Vortex Interaction Noise—Experimental and Mathematical Results," AIAA Paper 87-0251, 25th AIAA Aerospace Sciences Meeting, Reno, NV, January 12–15, 1987.
- ¹⁶George, R. E., and Duffy, V., "In-Flight Measurement of Aircraft Acoustic Signals," Proceedings of the 23rd International Instrumentation Symposium, Las Vegas, NV, 1977, Vol. 14.
- ¹⁷Boxwell, D. A., and Schmitz, F. H., "In-Flight Acoustic Comparison of the 540 and K747 Main Rotors for the AH-1S Helicopter," Production Validation Test-Government; Kafo, an K747 Improved Main Rotor Blade, USAAEFA Project No. 77-38, U.S. Army, October 1979, pp. 65–90.
- ¹⁸Schmitz, F. H., "Rotor Noise," in *Aeroacoustics of Flight Vehicles: Theory and Practice*, edited by H. Hubbard, NASA RP 1258, 1991; WRDC Technical Report 90-3052, August 1991.
- ¹⁹Homicz, G. F., and George, A. R., "Broadband and Discrete Frequency Radiation From Subsonic Rotors," *Journal of Sound & Vibration*, Vol. 36, (2), September 1974, pp. 151–177.
- ²⁰Brooks, T. F., Marcolini, M. A., and Pope, D. S., "Main Rotor Broadband Noise Study in the DNW," *Journal of the American Helicopter Society*, Vol. 34, (2), April 1989, pp. 3–12.
- ²¹Leverton, J. W., "The Noise Characteristics of a Large 'Clean' Rotor," *Journal of Sound & Vibration*, Vol. 27, (3), April 1973, pp. 357–376.
- ²²Gutin, L., "On the Sound Field of a Rotating Propeller," NACA TM 1195, 1948.
- ²³Deming, A. F., "Noise from Propellers with Symmetrical Sections at Zero Blade Angle, II," NACA TN 679, 1938.
- ²⁴Ffowcs Williams, J. E., and Hawkings, D. L., "Sound Generation by Turbulence and Surfaces in Arbitrary Motion," *Philosophical Transactions of Royal Society of London, Series A*, Vol. 264, (1151), May, 1969, pp. 321–342.
- ²⁵Farassat, F., "Theory of Noise Generation from Moving Bodies with an Application to Helicopter Rotors," NASA TR R-451, 1975.
- ²⁶Farassat, F., "Linear Acoustic Formulas for Calculation of Rotating Blade Noise," *AIAA Journal*, Vol. 19, (9), September 1981, pp. 1122–1130.
- ²⁷Brentner, K. S., "Prediction of Helicopter Rotor Discrete Frequency Noise—A Computer Program Incorporating Realistic Blade Motions and Advanced Acoustic Formulation," NASA TM-87721, 1986.
- ²⁸Sutton, C., Koushik, S., and Schmitz, F. H., "High Quality Acoustic Time History Measurements of Rotor Harmonic Noise in Confined Spaces," American Helicopter Society 69th Annual Forum Proceedings, Phoenix, AZ, May 21–23, 2013.
- ²⁹Schmitz, Fredric H., and Yu, Yung H., "Theoretical Modeling of High-Speed Helicopter Impulsive Noise," *Journal of the American Helicopter Society*, Vol. 24, (1), 1979, pp. 10–19.
- ³⁰Boxwell, D. A., Yu, Y. H., and Schmitz, F. H., "Hovering Impulsive Noise—Some Measured and Calculated Results," *Helicopter Acoustics*, NASA CP-2052, Part I, 1978, pp. 309–322.
- ³¹Yu, Y. H., Caradonna, F. X., and Schmitz, F. H., "The Influence of the Transonic Flow Field on High-Speed Helicopter Impulsive Noise," Proceedings of the Fourth European Rotorcraft and Powered Lift Aircraft Forum, Stresa, Italy, Vol. 2, September 13–15, 1978, pp. 58-0–58-16.

- ³²Kittleson, J. K., and Yu, Y. H., "Holographic Interferometry Technique for Rotary Wing Aerodynamics and Noise," NASA TM-84723, 1982.
- ³³Schmitz, F. H., and Yu, Y. H., "Helicopter Impulsive Noise: Theoretical and Experimental Status," *Journal of Sound & Vibration*, Vol. 109, (3), September 1986, pp. 361–422.
- ³⁴Strawn, R. C., Oliker, R., and Biswas, R., "New Computational Methods for the Prediction and Analysis of Helicopter Noise," *Journal of Aircraft*, Vol. 34, (5), September–October 1997, pp. 665–672.
- ³⁵di Francescantonio, P., "A New Boundary Integral Formulation for the Prediction of Sound Radiation," *Journal of Sound and Vibration*, Vol. 202, (4), 1997, pp. 491–509.
- ³⁶Schmitz, F. H., Aggarwal, H. R., and Boxwell, D. A., "Prediction and Measurement of Low-Frequency Harmonic Noise of a Hovering Model Helicopter Rotor," *Journal of Aircraft*, Vol. 37, (5), September–October 2000, pp. 786–795.
- ³⁷Kuo, B. C., Sim, B., and Schmitz, F.H., "Blade–Vortex Interaction Wave Radiation Patterns of Helicopter Blades with Different Leading-Edge Geometry," American Helicopter Society 58th Annual Forum Proceedings, Montréal, Quebec, Canada, June 11–13, 2002.
- ³⁸Schmitz, F. H., and Sim, B. W., "Acoustic Phasing and Amplification Effects of Single Rotor Helicopter Blade–Vortex Interactions," *Journal of the American Helicopter Society*, Vol. 46, (4), October 2001, pp. 273–282.
- ³⁹Beddoes, T. S., "A Wake Model for High Resolution Airloads," Second International Conference on Rotorcraft Basic Research, Research Triangle Park, NC, February 19–21, 1985.
- ⁴⁰Leishman, J. G., *Principles of Helicopter Aerodynamics*, Cambridge University Press, New York, NY, 2006, pp 457–489.
- ⁴¹Schmitz, F. H., Boxwell, D. A., Splettsstoesser, W. R., Schultz, K. J., Lewy, S., and Caplot, M., "Model Helicopter Rotor Aerodynamics and Acoustics as Measured in Two Anechoic Wind Tunnels," *Journal of Aircraft*, Vol. 37, (2), 2000, pp. 235–244.
- ⁴²Soderman, P. T., Schmitz, F. H., Allen, C. S., Jaeger, S. M., Sacco, J. N., and Hayes, J. A., "Design of a Deep Acoustic Lining for the 40- by 80- Foot Wind Tunnel Test Section," Fifth AIAA/CEAS Aeroacoustics Conference, Seattle, WA, May 10–12, 1999.
- ⁴³Yu, Y., Liu, S. R., Landgrebe, A. J., Lorber, P. F., Pollack, M. J., Martin, R. M., and Jordan, D., "Aerodynamic and Acoustic Test of a United Technologies Model Scale Rotor at DNW," American Helicopter Society 64th Annual Forum Proceedings, Washington, DC, April 29–May 1, 1990.
- ⁴⁴Ananthan, S., Baeder, J. D., Sitaraman, J., Hahn, S., and Iacarino, G. "Hybrid Unsteady Simulation of Helicopters: HUSH," 26th AIAA Applied Aerodynamics Conference, Honolulu, HI, August 18–21, 2008.
- ⁴⁵Koushik, S., and Schmitz, F., "Design of Gust Generator to Study Impulsive Noise Radiation Due to Helicopter Blade–Vortex Interaction," American Helicopter Society Fourth Decennial Specialists' Meeting on Aeromechanics, San Francisco, CA, January 21–23, 2004.
- ⁴⁶Koushik, S., Schmitz, F., and Sim, B., "Towards the Understanding of BVI Noise through Experimental Simulation," American Helicopter Society 62nd Annual Forum Proceedings, Phoenix, AZ, May 9–11, 2006.
- ⁴⁷Koushik, S., and Schmitz, F. H., "A New Experimental Approach to Study Helicopter Blade–Vortex Interaction Noise," 14th AIAA/CEAS Aeroacoustics Conference, Vancouver, Canada, May 5–7, 2008.
- ⁴⁸Koushik, S., and Schmitz, F., "An Experimental and Theoretical Study of Blade–Vortex Interaction Noise," *Journal of the American Helicopter Society*, **58**, 032006 (2013).
- ⁴⁹Gervais, M., and Gareton, V., "Analysis of Main Rotor Noise Reduction due to Novel Planform Design—The Blue Edge™ Blade," 37th European Rotorcraft Forum, Gallarate, Italy, September 13–15, 2011.
- ⁵⁰Kuo, B. C., Sim, B. W., and Schmitz, F. H., "Blade–Vortex Interaction Wave Radiation Patterns of Helicopter Blades with Different Leading-Edge Geometry," American Helicopter Society 58th Annual Forum Proceedings, Montréal, Quebec, Canada, June 11–13, 2002.
- ⁵¹Brooks, T. F., "Wavy-Planform Helicopter Blades Make Less Noise," NASA Tech Brief 20110016725, February 2004.
- ⁵²Feinerman, J., Koushik, S., and Schmitz, F. H., "Effect of Leading-Edge Serrations on Helicopter Blade–Vortex Interaction Noise," American Helicopter Society 67th Annual Forum Proceedings, Virginia Beach, VA, May 3–5, 2011.
- ⁵³Schmitz, F. H. "Reduction of Blade–Vortex Interaction (BVI) Noise through X-Force Control," *Journal of the American Helicopter Society*, Vol. 43, (1), January 1998, pp. 4–24.
- ⁵⁴Schmitz, F. H., Gopalan, G., and Sim, B. W., "Flight Path Management/Control Methodology to Reduce Helicopter Blade–Vortex (BVI) Noise," *Journal of Aircraft*, Vol. 39, (2), March 2002, pp. 193–205.
- ⁵⁵Hawles, D. R., "Flight Operations to Minimize Noise," Proceedings of the American Helicopter Society-AIAA-University of Texas at Arlington Joint Symposium on Environmental Effects of VTOL Designs, Arlington, TX, Nov 16–18, 1970; *Vertiflite*, Vol. 17, (1), February 1971, pp. 4–9.
- ⁵⁶Cox, C., Leverton, J., et al., "Fly Neighborly Guide," Fly Neighborly Committee of Helicopter Association International (HAI), 2013.
- ⁵⁷Sim, B., Beasman, T., Schmitz, F. H., and Gopalan, G., "In-Flight Blade–Vortex Interaction (BVI) Noise Measurements Using a Boom-Mounted Microphone Array," American Helicopter Society 60th Annual Forum Proceedings, Baltimore, MD, June 7–10, 2004.
- ⁵⁸Schmitz, F. H., Greenwood, E., Sickenberger, R., and Gopalan, G., "Measurement and Characterization of Helicopter Noise in Steady-State and Maneuvering Flight," American Helicopter Society Annual Forum Proceedings, Virginia Beach, VA, May 1–3, 2007.
- ⁵⁹Jacobs, E. "S76 Terminal Approach Noise Abatement," HAI Heli-Expo Fly Neighborly Workshop, Las Vegas, NV, 2006.
- ⁶⁰Schmitz, F. H., and Gopalan, G., "High-Speed Impulsive Helicopter Noise Reduction Possibilities through on-Blade Acoustic Control," International Forum on Rotorcraft Multidisciplinary Technology Organized by AHS International and the Korean Society for Aeronautical and Space Sciences, Seoul, Korea, October 15–17, 2007.
- ⁶¹Gopalan, G., and Schmitz, F. H., "Understanding Far Field Near-in-Plane High Speed Harmonic Helicopter Rotor Noise in Hover: Governing Parameters and Active Acoustic Control Possibilities," Proceedings of the AHS Specialist's Conference on Aeromechanics, San Francisco, CA, January 23–25, 2008.
- ⁶²Gopalan, G., and Schmitz, F. H., "Far-Field Near-in-Plane Harmonic Main Rotor Helicopter Impulsive Noise Reduction Possibilities," Proceedings of the AHS Annual Forum and Technology Display, Montreal, Canada, April 29–May 1, 2008.
- ⁶³Sim, B. W., Janakiram, R. D., and Lau, B. H., "Reduced In-Plane, Low-Frequency Noise of an Active Flap Rotor," *Journal of the American Helicopter Society*, **59**, 022002 (2014).
- ⁶⁴Sargent, D. C., Gopalan, G., and Schmitz, F. H., "Acoustic Design and Parametric Variations, Active Acoustic Control, and Performance Study of In-Plane Far-Field Helicopter Rotor Noise in Forward Flight," American Helicopter Society 69th Annual Forum Proceedings, Phoenix, AZ, May 2010.
- ⁶⁵Sargent, D. C., "Active Jet Acoustic Control of Low Frequency, In-Plane Helicopter Harmonic Noise," Ph.D. Dissertation, University of Maryland, College Park, MD, 2012.

Fredric H. Schmitz is currently a part-time Senior Research Professor in the Aerospace Department at the Alfred E. Gessow Rotorcraft Center at the University of Maryland. Dr. Schmitz has more than 50 years of experience in aeronautics, specializing in fundamental research and technical management. His research career began in industry (Boeing Vertol), working with W. Z. Stepniewski (the first Nikolsky lecturer) on rotorcraft optimal performance and control problems, including trying to determine how to fly Vietnam-era rotorcraft quietly. His fundamental research work on rotorcraft acoustics began when he accepted a position with the Army Aeronautical Research Laboratory at NASA Ames Research Center at Moffett Field, CA. In that job, he pioneered the use and development of specialized worldwide facilities to validate and develop new computer modeling approaches to rotorcraft noise. Dr. Schmitz also worked as a part-time Consulting Professor at Stanford University, where he developed and taught a sequence of rotorcraft classes. He then became the Army Fluid

Dynamics Division Chief at Ames for a few years before moving to a NASA SES position to head up the newly formed National Full-Scale Aerodynamics Complex, consisting of 40×80 -foot and 80×120 -foot wind tunnels. After several successful years in that position, he was selected to become the Director of Aeronautics at NASA Ames. In 1998, he retired from government service and joined the faculty at the University of Maryland as the Martin Professor of Rotorcraft Acoustics. Since then, he has built a rotorcraft acoustic program at UMD that utilizes fundamental experiments (ground and flight test) to validate key aspects of acoustic theory. Dr. Schmitz has a BAE degree from RPI and Master's and Ph.D. degrees from Princeton University, and he has authored more than 50 archival publications, including three book chapters. He is a Fellow of the AHS and the AIAA, has won many national awards and honors, and has a commercial rotary-wing pilot's license.